CRREL
REPORT 79-7

Penetration tests in subsea permafrost, Prudhoe Bay, Alaska

CRREL Report 79-7

Penetration tests in subsea permafrost, Prudhoe Bay, Alaska

S.E. Blouin, E.J. Chamberlain, P.V. Sellmann and D.E. Garfield

May 1979

Prepared for
DEPARTMENT OF COMMERCE
NATIONAL OCEANIC AND ATMOSPHERIC ADMINISTRATION/ERL
By
UNITED STATES ARMY
CORPS OF ENGINEERS
COLD REGIONS RESEARCH AND ENGINEERING LABORATORY
HANOVER, NEW HAMPSHIRE, U.S.A.

Unclassified

SECURITY CLASSIFICATION OF THIS PAGE (When Data Entered)

REPORT DOCUMENTATION PAGE

READ INSTRUCTIONS BEFORE COMPLETING FORM

1. REPORT NUMBER: CRREL Report 79-7

2. GOVT ACCESSION NO.:

3. RECIPIENT'S CATALOG NUMBER:

4. TITLE (and Subtitle): PENETRATION TESTS IN SUBSEA PERMAFROST, PRUDHOE BAY, ALASKA

5. TYPE OF REPORT & PERIOD COVERED:

6. PERFORMING ORG. REPORT NUMBER:

7. AUTHOR(s): S.E. Blouin, E.J. Chamberlain, P.V. Sellmann and D.E. Garfield

8. CONTRACT OR GRANT NUMBER(s): Order No. 01-5-022-2313

9. PERFORMING ORGANIZATION NAME AND ADDRESS: U.S. Army Cold Regions Research and Engineering Laboratory, Hanover, New Hampshire 03755

10. PROGRAM ELEMENT, PROJECT, TASK AREA & WORK UNIT NUMBERS:

11. CONTROLLING OFFICE NAME AND ADDRESS: Department of Commerce, National Oceanic and Atmospheric Administration/ERL, Boulder, Colorado

12. REPORT DATE: May 1979

13. NUMBER OF PAGES: 49

14. MONITORING AGENCY NAME & ADDRESS (if different from Controlling Office):

15. SECURITY CLASS. (of this report): Unclassified

15a. DECLASSIFICATION/DOWNGRADING SCHEDULE:

16. DISTRIBUTION STATEMENT (of this Report)

Approved for public release; distribution unlimited.

17. DISTRIBUTION STATEMENT (of the abstract entered in Block 20, if different from Report)

18. SUPPLEMENTARY NOTES

This study was funded by the Bureau of Land Management, U.S. Department of the Interior, through the Department of Commerce.

19. KEY WORDS (Continue on reverse side if necessary and identify by block number)

Penetration tests
Prudhoe Bay, Alaska
Subsea permafrost

20. ABSTRACT (Continue on reverse side if necessary and identify by block number)

Sediments beneath the Beaufort Sea near Prudhoe Bay, Alaska, were probed at 27 sites using a static cone penetrometer to determine engineering properties and distribution of material types, including ice-bonded sediments. The probe provided both point and casing resistance data and thermal profiles. At five sites these data were correlated with information from adjacent drilled and sampled holes. These control data and the quality of the probe information permitted profiles of sediment type and occurrence of ice-bonded material to be developed along three lines that included various geological features and depositional environments. Material properties were quite variable in the upper 14 m of sediments probed. In general, softer, finer-grained sediments occurred in the upper layers, while penetration refusal was met in stiff gravels 10 to 12 m below the seabed. Seabed temperatures during the study were all below 0°C.

DD FORM 1 JAN 73 1473 EDITION OF 1 NOV 65 IS OBSOLETE

Unclassified

SECURITY CLASSIFICATION OF THIS PAGE (When Data Entered)

20. Abstract (cont'd)

However, because of uncertainties in freezing point values caused by brines, evaluation of the penetration resistance data was required to identify the occurrence of ice-bonded sediments. The coupling of thermal and penetration resistance data revealed that seasonally ice-bonded sediments occurred where the sea ice froze back to or near the seabed. Deeper, perennially frozen sediments also appeared to be present at several probe sites. The penetration data obtained can be used to aid in the design of shallow and deep foundations in both ice-bonded and unfrozen subsea sediments.

PREFACE

This report was prepared by the following members of the U.S. Army Cold Regions Research and Engineering Laboratory: S.E. Blouin, Research Civil Engineer, and E.J. Chamberlain, Research Civil Engineer, of the Applied Research Branch, and P.V. Sellmann, Geologist, of the Geotechnical Research Branch, all of the Experimental Engineering Division; and D.E. Garfield, Mechanical Engineer, of the Engineering and Measurement Services Branch, Technical Services Division.

Funding for this study was provided by the Bureau of Land Management, through the Department of Commerce, National Oceanic and Atmospheric Administration/ERL, Outer Continental Shelf Environmental Assessment Program Office, Boulder, Colorado, under Order No. 01-5-022-2313, *Delineation and Engineering Characteristics of Permafrost Beneath the Beaufort Sea, Alaska* (RU-105).

H.T. Ueda and D.M. Cole of CRREL reviewed the technical content of this report.

The authors thank Dr. D.M. Hopkins of the U.S. Geological Survey for his constructive comments and cooperation in this project.

CONTENTS

ILLUSTRATIONS

TABLES

PENETRATION TESTS IN SUBSEA PERMAFROST, PRUDHOE BAY,ALASKA

S.E. Blouin, E.J. Chamberlain
P.V. Sellmann and D.E. Garfield

INTRODUCTION

This study was part of a larger project undertaken to delineate the occurrence of subsea permafrost in the Prudhoe Bay area of the Beaufort Sea and to define its engineering properties. It was sponsored by the Bureau of Land Management and directed by the National Oceanic and Atmospheric Administration, as part of their joint Outer Continental Shelf Environmental Assessment Program. The bulk of the effort was spent on a two-year drilling and laboratory program which provided core and data from nine sites within and adjacent to Prudhoe Bay to depths of nearly 70 meters. Details of this program have been reported by Chamberlain et al. (1978) and Sellmann et al. (1978).

The penetration program was a two-year ancillary effort intended to develop equipment and techniques for rapidly obtaining engineering properties and temperature profiles of subsea sediments and for identifying shallow, ice-bonded permafrost. Results of the 1976 pilot study were reported by Chamberlain et al. (1978). Both static and dynamic penetration tests were run at four sites, three of which were adjacent to drilling sites. Good correlation was obtained between the static and dynamic penetration resistances and sediment types determined from the drill core logs.

Convinced by these results that the potential utility of the penetrometer was high, the investigators of the present study decided to develop a new penetrometer for the 1977 field season that would eliminate the major difficulties encountered with the prototype equipment. These difficulties included long setup and testing times, lack of an automated data acquisition system, operator discomfort because of lack of protection from the elements, and inadequate loading capacity of the equipment.

This report describes the penetrometer used to conduct this investigation, test procedures, and methods of data collection and reduction. It correlates the results with laboratory tests and presents conclusions based on the study.

EQUIPMENT

The equipment developed for the second year's program was designed for rapid, automated acquisition of engineering data, including temperature profiles. The primary mode of testing was intended to be static with a supplementary dynamic capability planned for use beyond the limits of the static loading. Penetrometer data were eventually collected from 27 sites along four lines, three of which extended from the coast into the Beaufort Sea with the

fourth running offshore roughly perpendicular to them. A detailed description of the entire apparatus and its operation is given in Appendix A; a brief description is given below.

The testing equipment (Fig. 1) was completely housed in a 1.5-m×2.6-m×2.3-m (5-ft×8½-ft×7½-ft) building mounted on a ski base. The skis also served as a parking pad for the large crawler tractor that acted as the reaction force for testing and eliminated the time-consuming anchor setting procedures employed during the first season (Fig. 2). The tractor was also used to transport the sled-mounted penetrometer. The heated building contained all the equipment necessary for electrical data acquisition and provided a comfortable working environment for the operators. In the static mode, shown schematically in Figure 1, the probe was pushed into the sea floor by means of a 12.7-cm (5-in.)-diameter hydraulic ram mounted atop the equipment building. Standard AW drill rod and casing were used to advance the probe and the casing shoe. The 1.83-m (6-ft) cylinder stroke allowed use of 1.52-m (5-ft) standard sections of drill rod and casing.

The 6.35-cm (2½-in.)-diameter probe point, shown in Figure 3, was attached to the AW rod, while the casing was used to push the friction shoe and to isolate the point and rod from friction forces that would have otherwise caused an apparent increase in point resistance. The cylindrical casing shoe has the same diameter as the point and is attached to the casing behind the point shroud. The shoe was designed to measure local sidewall friction behind the point. The tapered shroud behind the point allowed relative motion between the point and casing while preventing soil from being forced into the annulus between the rod and casing, which was a major problem during the 1976 field season. The probe design is similar to the Dutch "mantle cone" described by Heijnen (1974).

The hydraulic ram, pressurized with an electrically powered hydraulic pump, was capable of driving the probe at a maximum velocity of approximately 2 cm/sec (0.8 in./sec). Electrical power for the hydraulic pump, lighting and instrumentation was provided by a diesel generator mounted along with the pump in an enclosure on the front of the building (Fig. 1). Cooling air from the generator was used to heat the building.

In the dynamic mode, the probe was intended to be driven by a hydraulically-actuated hammer having a 590-kg (1300-lb) drop weight with a 0.3-m (12-in.) free fall. A heavy weight and short fall were utilized to minimize flow interference in the hydraulic system and to reduce transient peak stresses in the hammer anvil and probe stem. The driving frequency was adjustable up to approximately 30 blows per minute. A series of mechanical problems (see App. A), and the fact that the driving energy appeared to be too low to advance the probe significantly once it had reached static refusal, caused the dynamic mode of operation to be completely abandoned after several unsuccessful attempts.

DATA COLLECTION AND REDUCTION

The total resistance of the drill rod and casing and the casing resistance alone were plotted continuously as functions of displacement on an X-YY recorder. These data were obtained from load cells built into the coupler joining the probe string to the hydraulic ram. Displacement was measured with a cable-actuated linear displacement transducer attached between one of the overhead support beams and the end of the cylinder rod. An example of a plot from the recorder from the 7.3-to 10.4-m (24-to 34-ft) depth at probe site PH-10 is shown in Figure 4. On the left hand side of the original plot, total resistance was plotted at a scale of 715 kg/cm (4000 lb/in.). On the right hand side, casing resistance was shown on a scale of 358 kg/cm (2000 lb/in.). The depth scale was 10 cm/cm (10 in./in.); therefore, each data plot contained 3.05 m (10 ft) of data, the output from advancing two 1.52-m (5-ft) lengths of probe string.

In order to reduce these plots to useable size, they were digitized at the rate of 1 bit per 2.5 cm (1 in.) of depth and replotted by computer at a reduced scale. The plot of the entire hole at site PH-10 is shown in Figure 5. The static cone (or point) resistance q_c, in bars, is plotted as a function of depth along with the local skin friction f_s. The cone resistance is simply the point load (obtained by subtracting the casing load from the total load) divided by the 31.7-cm² (4.91-in.²) projected area of the point. The local skin friction is the casing load divided by the 304.0-cm² (47.12-in.²) area of the cylindrical casing shoe. Inherent in this calculation is the assumption that all the casing load results from skin friction on the shoe alone. The implications of this assumption are discussed in the section on data interpretation. However, it appears that occasionally

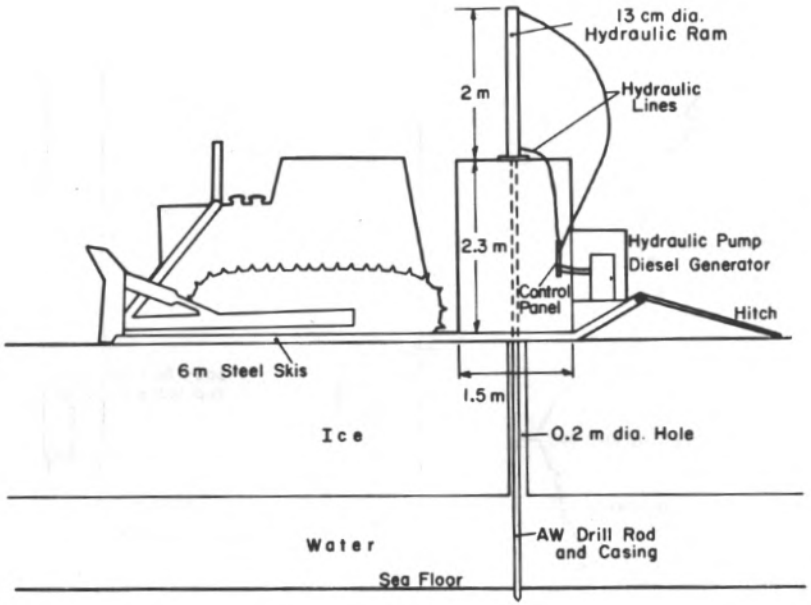

Figure 1. Schematic of static penetrometer apparatus used during the 1977 field season.

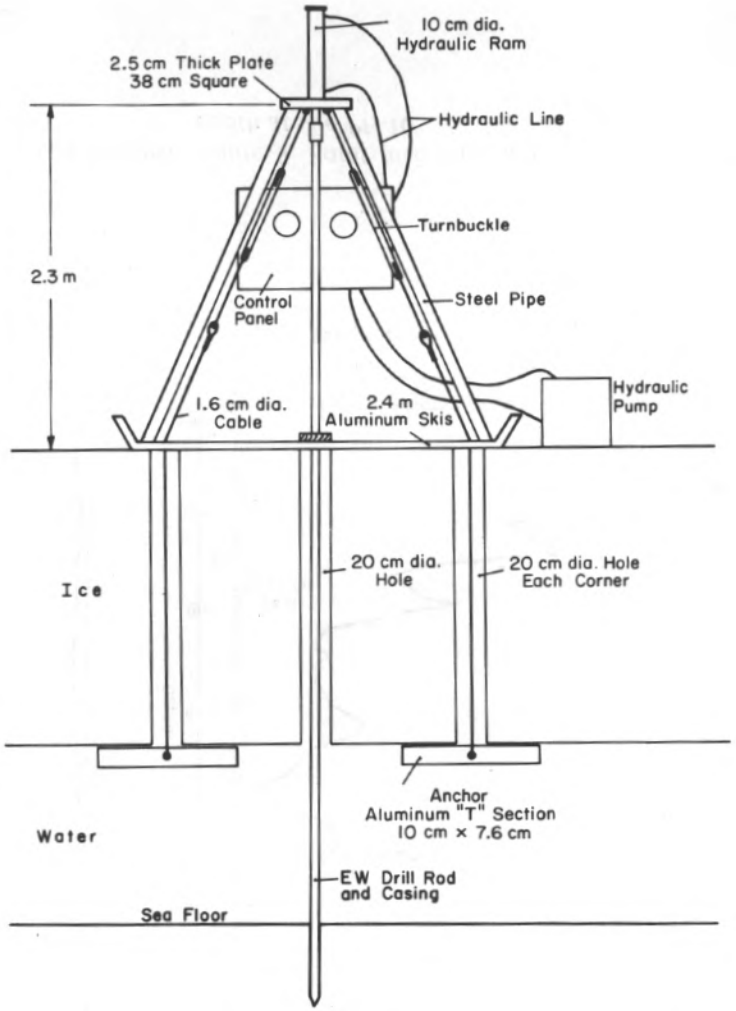

Figure 2. Schematic of static penetrometer apparatus used during the 1976 field season.

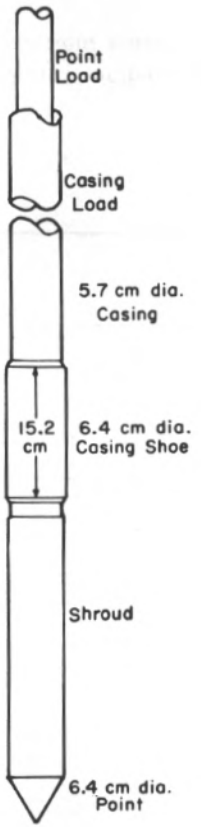

Figure 3. Schematic of probe point and casing.

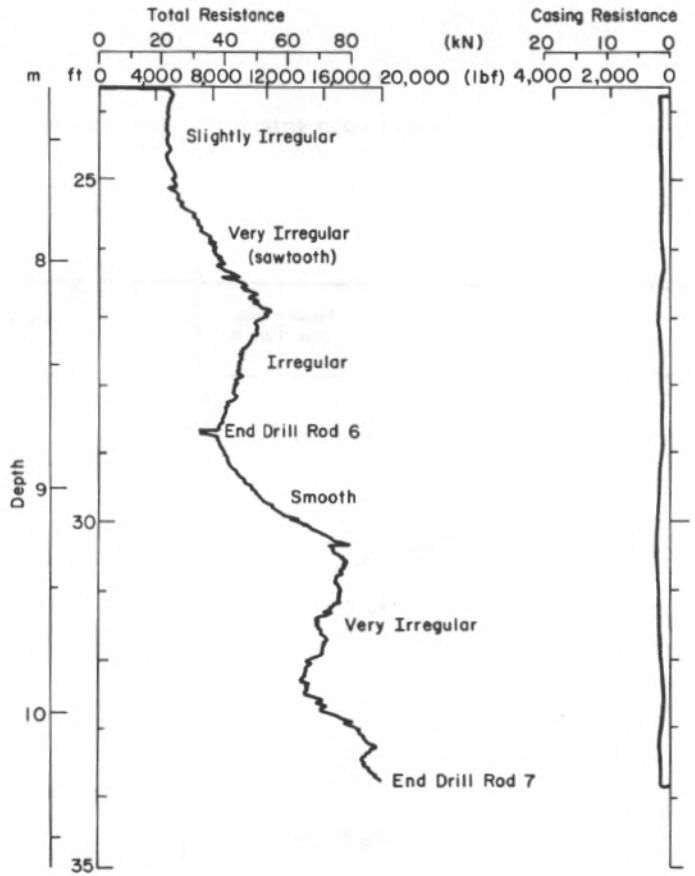

Figure 4. Example of data output on recorder at site PH-10.

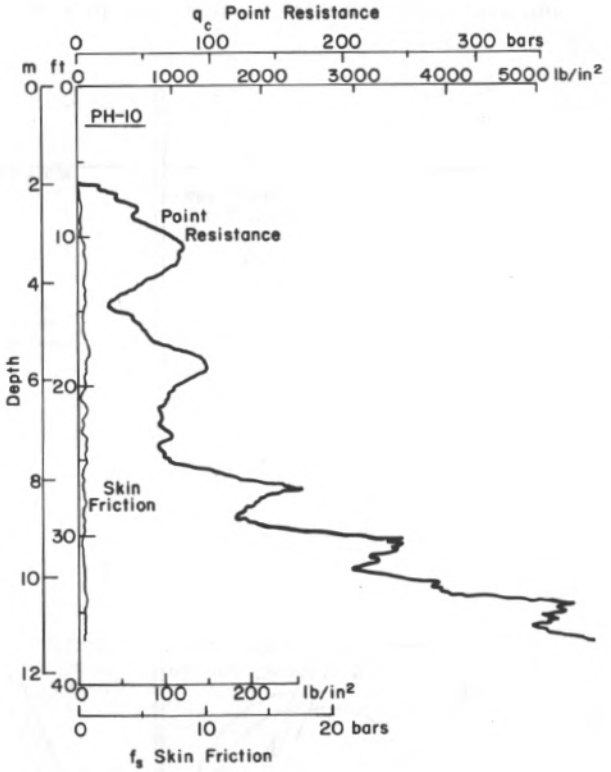

Figure 5. Point resistance and skin friction versus depth at site PH-10.

additional side friction on the casing itself results from collapse of the probe hole around the casing above the point and shoe assembly.

The reduced plots of point resistance and skin friction from the 27 probe sites studied during the 1977 season are presented in Appendix B. The probe sites studied were designated PH-1 through PH-27 and their locations along with those of the drill sites (PB-1 through PB-8) are shown on the map in Figure 6. The site coordinates are listed in Table 1, along with data on ice thickness, water depth and maximum depth of penetration. The maximum depth of penetration was determined by the reaction load capacity of the probe sled. When a total load on the probe string reached the design limit of 124.5 kN (28,000 lb), the test was terminated. If this entire load was borne on the point, the static point resistance was 393 bars (5700 lb/in.^{2}).

The probe sites were selected in an attempt to obtain data from most of the depositional environments in the Prudhoe area. As shown in Figure 6, data were collected from three lines normal to the coast. The shortest and westernmost line (4) was off Stump Island in an offshore bar environment. The middle line (2), along which some of the 1976 season's drilling and probing was conducted, was previously established by Osterkamp and Harrison (1976). It extended true north offshore from the ARCO discovery well near the west ARCO dock. The first line (1) ran northwesterly on the east side of Gull Island and included the first drill holes from both the 1976 and 1977 drilling seasons. A fourth survey line (3) ran roughly perpendicular to these three lines, extending along the 2-m bathymetric contour from Stump Island to the Sagavanirktok River Delta.

Temperature data were obtained in the bore of the drill rod after the penetrometer had been driven to the maximum possible depth. The rod was filled with a nonfreezing fluid and a thermistor probe was lowered to the bottom. Thermal equilibrium was observed to occur in 6 to 8 hours. To ensure that thermal equilibrium did, in fact, occur before the temperature readings were made, the probe was allowed to remain in place over night. Whenever two penetration tests were conducted in a single day, temperatures were obtained only at the second site. Measurements were normally taken at 1.5-m (5-ft) depth intervals from the bottom up. In the upper portion of the profile, where the temperature at some sites increased rapidly with depth, temperature observations were made at closer intervals.

Five to twenty minutes were usually allowed for the thermistor probe to reach equilibrium after being raised to a new position; the time required was dependent on the size of the temperature change. The resistance of the thermistor probe was continuously displayed on a digital ohmmeter so that temperature changes could be readily observed.

The equilibrium temperature for each measurement was established in terms of the measured thermistor resistance as the resistance where less than a 1-ohm change occurred in one minute. For the thermistor probes employed, a 1-ohm change is approximately equal to 0.0035°C (0.0063°F).

Plots of the temperature profiles along each of the three major survey lines (lines 1, 2 and 3) are shown in Figures 7-9. In some cases where the temperature change with depth was very rapid, such as near the top of site PH-27 (Fig. 9), convection cells were set up in the bore fluid. Temperature fluctuations as large as 0.05°C (0.09°F) were observed to occur as a result of the convection. In the few cases where this occurred, the reported temperatures are average values.

DATA ANALYSIS AND INTERPRETATION

Point penetration resistance and material properties

A summary of the cone penetration resistance values for each of the major study lines is given in Figure 10. Maximum and minimum penetration resistance values are given for 2-m increments. With a few exceptions penetration resistance values are low in the upper few meters and reach, or nearly reach, refusal (395 bars) at depths between 10 and 14 m below the seabed. This refusal value was not always achieved because in most cases the resistance level rose rapidly as refusal was approached, requiring the operator to reduce the hydraulic pressure to avoid damaging the equipment.

The spread between maximum and minimum penetration resistance values was narrow in the upper 4 m, compared with the wide range of values observed in the material below. It was found that variations in the resistance data

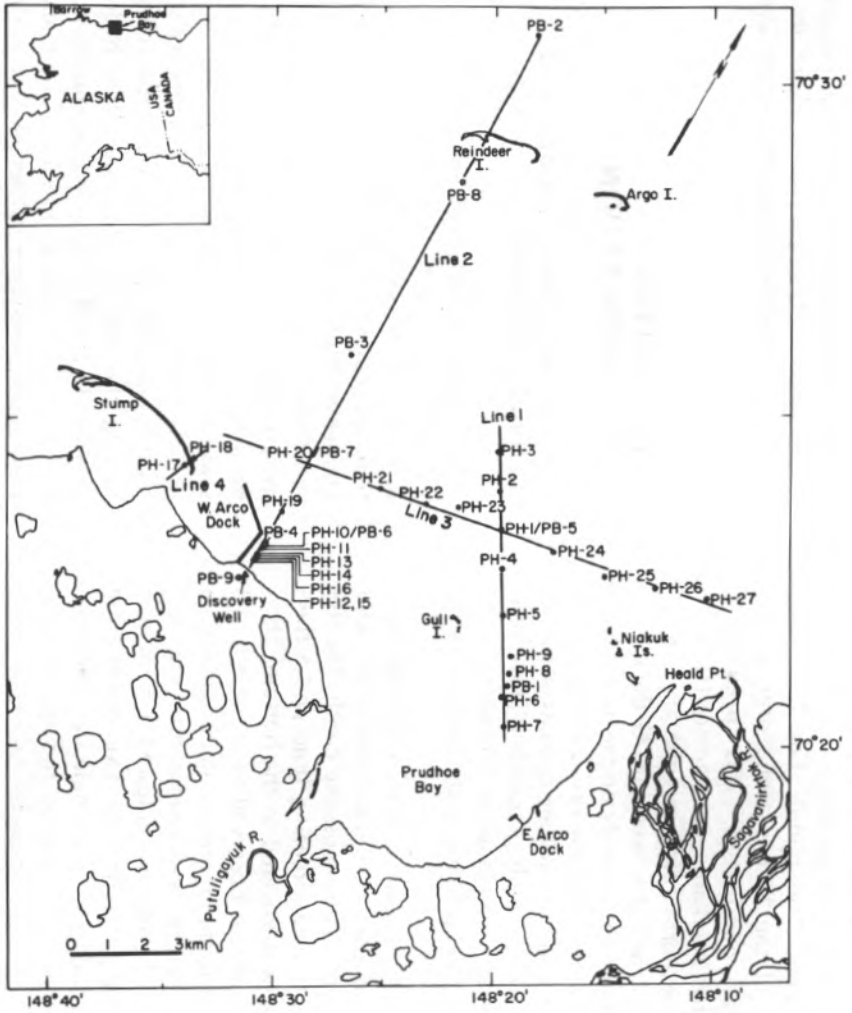

Figure 6. Map of site locations. PB-Drill sites; PH-Probe sites.

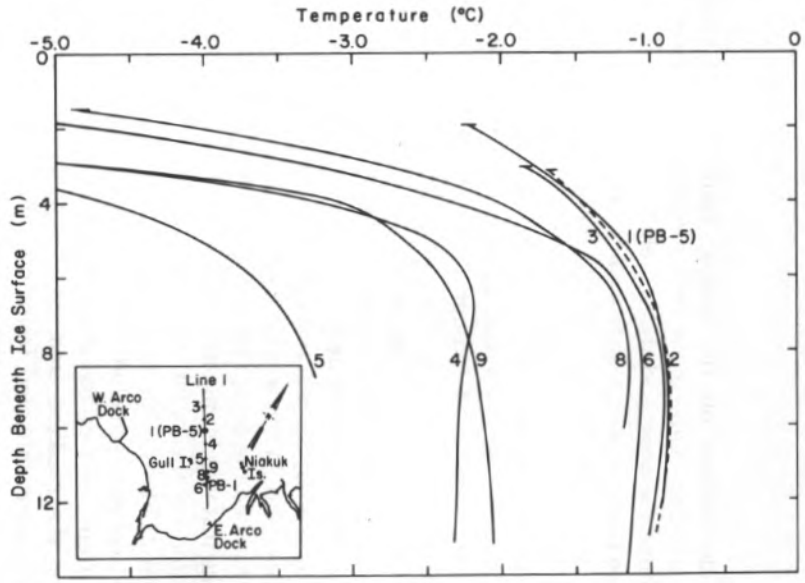

Figure 7. Temperature profiles, line 1. Numbers adjacent to curves indicate probe sites (PH). PB refers to drill sites.

Table 1. 1977 Prudhoe Bay CRREL probe locations.

Hole	General location	Latitude	Longitude	Ice thickness (m)	Water depth (m)	Maximum penetration (m)
PH-1	2.8 km NE of Gull Island	70°23.3′	148°19.7′	1.83	1.98	11.8
PH-2	3.7 km NE of Gull Island	70°23.85′	148°18.8′	1.83	3.15	12.3
PH-3	4.7 km NNE of Gull Island	70°24.4′	148°19.85′	1.52	3.23	12.9
PH-4	1.9 km NE of Gull Island	70°22.7′	148°19.7′	1.52	1.52	13.3
PH-5	1.4 km E of Gull Island	70°21.9′	148°19.6′	0.90	0.90	7.5
PH-6	3.3 km SSE of Gull Island	70°20.7′	148°19.7′	1.75	2.93	14.1
PH-7	2.6 km SSE of Gull Island	70°20.3′	148°19.5′	1.60	2.43	15.1
PH-8	2.6 km SE of Gull Island	70°21.2′	148°19.3′	1.50	1.69	10.3
PH-9	2.2 km SE of Gull Island	70°22.55′	148°31.9′	1.28	1.28	15.4
PH-10	1.0 km NE of Discovery Well	70°23.05′	148°30.6′	1.68	2.12	11.3
PH-11	0.8 km NE of Discovery Well	70°22.95′	148°30.8′	1.68	1.73	12.3
PH-12	0.5 km NE of Discovery Well	70°22.85′	148°31′	0.91	0.91	1.3
PH-13	0.63 km NE of Discovery Well	70°22.95′	148°30.9′	1.56	1.56	8.4
PH-14	0.57 km NE of Discovery Well	70°22.9′	148°30.9′	1.53	1.53	12.2
PH-15	0.5 km NE of Discovery Well	70°22.85′	148°31′	0.69	0.69	1.2
PH-16	0.54 km NE of Discovery Well	70°22.87′	148°31′	1.35	1.35	9.9
PH-17	0.12 km inland from Stump Is.	70°22.25′	148°34.1′	0.91	0.91	4.5
PH-18	0.12 km seaward from Stump Is.	70°24.3′	148°33.7′	1.83	1.94	11.3
PH-19	2.0 km NE of Discovery Well	70°23.5′	148°29.75′	1.80	1.95	10.6
PH-20	3.5 km NE of Discovery Well	70°24.25′	148°28.5′	1.80	2.06	11.1
PH-21	4.2 km NW of Gull Island	70°23.9′	148°25.3′	1.70	1.88	8.3
PH-22	3.3 km NW of Gull Island	70°23.65′	148°23.2′	1.85	2.17	10.9
PH-23	3.2 km N of Gull Island	70°23.6′	148°21.7′	1.60	2.13	11.2
PH-24	3.2 km NW of Niakuk Island	70°22.9′	148°17.3′	1.80	2.03	10.7
PH-25	1.5 km N of Niakuk Island	70°22.6′	148°15′	1.80	2.00	11.6
PH-26	1.9 km NE of Niakuk Island	70°22.4′	148°12.7′	1.80	1.83	10.0
PH-27	2.5 km NE of Heald Point	70°22.2′	148°10.4′	1.65	1.89	14.6

Note: 1 m = 3.28 ft.

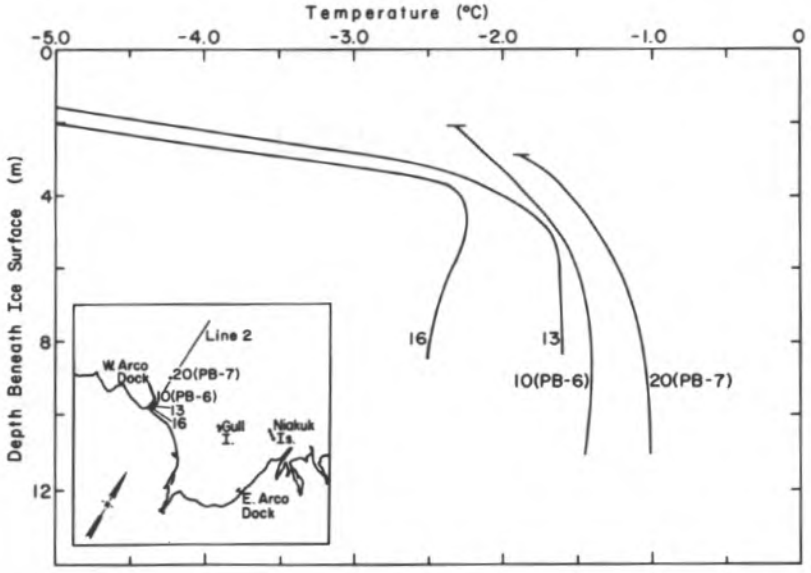

Figure 8. Temperature profiles, line 2.

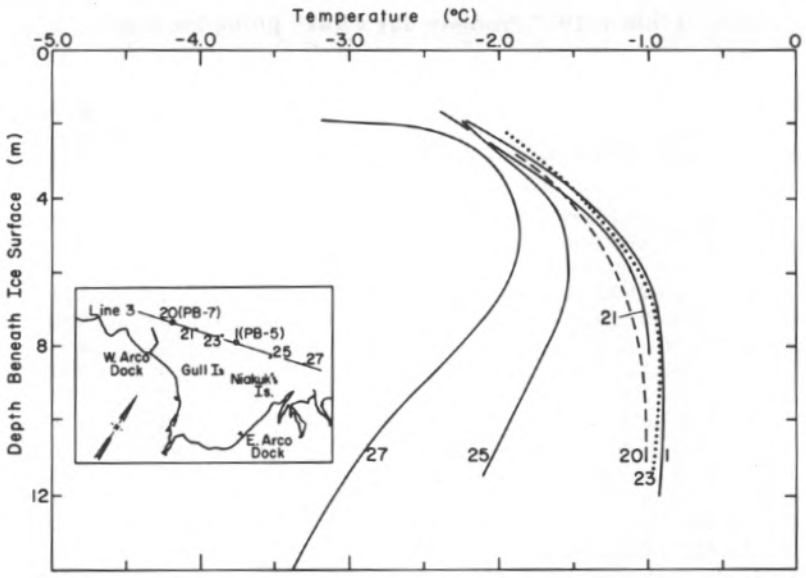

Figure 9. Temperature profiles, line 3.

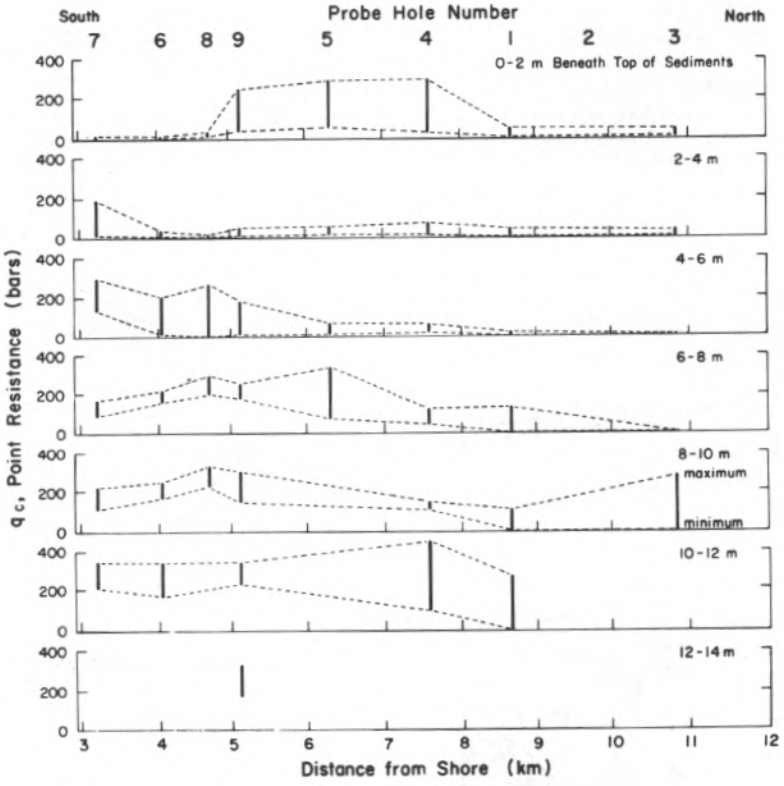

a. Line 1

Figure 10. Summary of point penetration resistance values along study lines. (1 bar = 14.5 lbf/in²; 1 km = 0.62 mile)

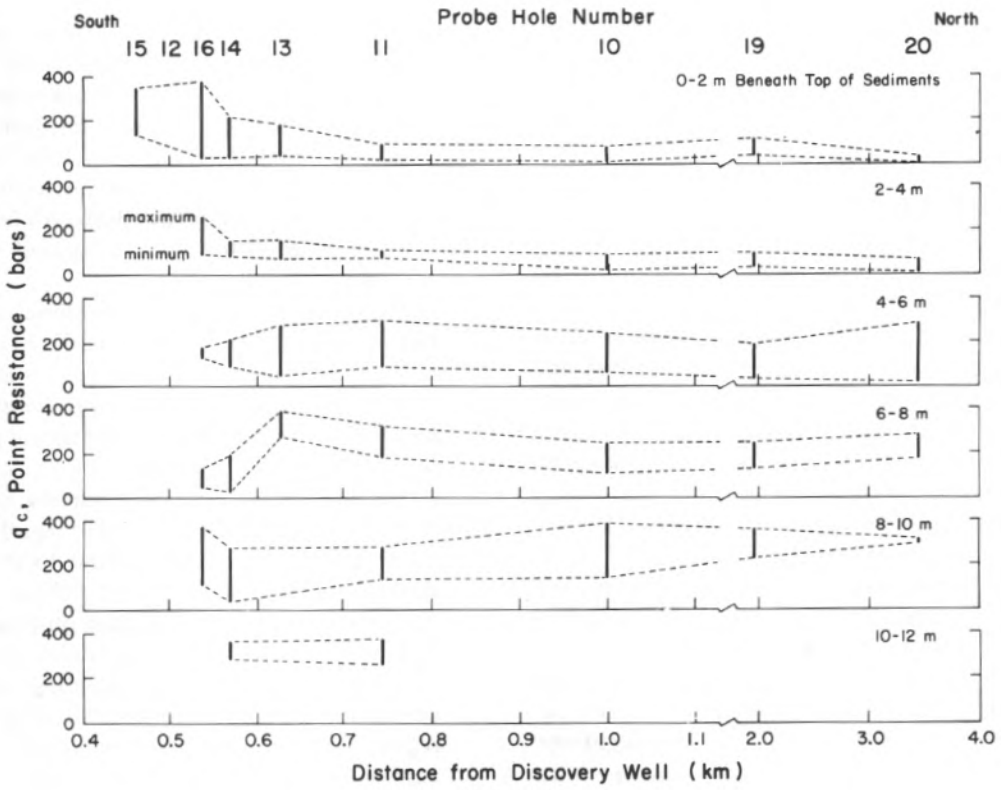

b. Line 2

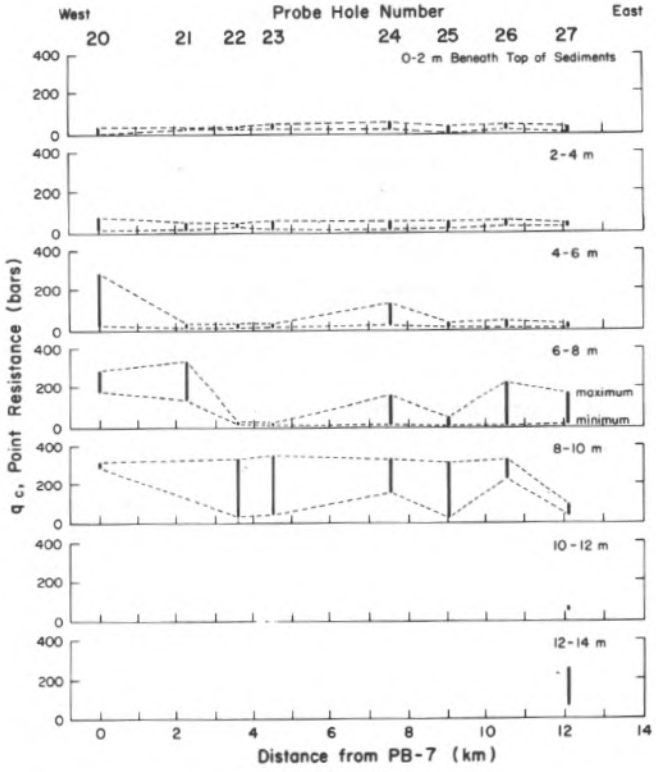

c. Line 3

Figure 10 (cont'd).

could be readily correlated with geologic features and the occurrence of frozen material. While very high penetration resistances caused the termination of probing at all sites (in contrast to running out of drill rod or encountering mechanical problems), the possibility of encountering finer-grained and softer materials at greater depths should not be discounted.

The speed and ease of obtaining this information permitted closely spaced observations and enabled detailed lateral variations to be interpolated along study lines. A comparison of point resistance data with logs from five drilled and sampled holes indicated that point resistance combined with certain characteristics of the continuous recorder plots correlated well with sediment type.

This observation was consistent with observations reported by Sanglerat (1972) in his book, *The Penetrometer and Soil Exploration*. However, Sanglerat reports that the ratio of the skin friction component to the penetration resistance is also essential to classify sediment types more accurately. Unfortunately, the skin friction component recorded during these investigations, while essential to separating the point penetration resistance from the total penetration resistance, appears to be of questionable value in determining this ratio because of the collapse or partial collapse of the sediments around the drill rod. This problem will be discussed in detail later in this report.

Fortunately, ground truth data obtained from the drill holes fill the information gap left by the uncertainties in the skin friction observation.

Point resistance was generally lower in the fine-grained sediments than in the coarse-grained sediments. Typically, point resistance varied in the fine-grained sediment from less than 0.01 bars (0.15 lb/in.^{2}) (at times insufficient to keep the point from advancing under the weight of the probe stem alone) to 15 bars (220 lb/in.^{2}). Resistance in the coarse-grained sediments varied continuously and often dramatically; the variations appeared to depend on grain size distribution and relative density. Resistances as low as 27.5 bars (400 lb/in.^{2}) were common, ranging upward to the capacity of the equipment (395 bars or 5730 lb/in.^{2}).

An example of the correlation of point resistance with sediment type is shown in the comparison of point resistance data from site PH-10 with the log from the adjacent borehole, PB-6A (Fig. 11). In general, higher point resistances correlate with layers of coarser material. Additionally, various investigators (e.g. Sanglerat 1972) have demonstrated that the higher the relative density in a given coarse-grained material, the higher is the corresponding point resistance. Thus, a loose, silty sand would be expected to have a point resistance toward the lower end of the spectrum, while the point resistance of dense, coarse gravel would lie toward the upper end.

Additional indicators of material type were the sounds and vibrations made as the probe point penetrated coarse-grained material and the resultant irregularities produced on the recorder plot of total load. When the probe was penetrating granular material, a continuous chain of acoustic emissions varying in intensity from barely audible to rather loud resulted. These sounds were very similar to those heard during high-pressure triaxial shear tests on granular soils. The penetration plot varied from a smooth to a very irregular (sawtooth) line, with greatest irregularity corresponding to greatest acoustic emission intensity. The degrees of irregularity and sound intensity are believed to be associated with intergranular stress concentrations that resulted either in the crushing or shearing of individual grains, or abrupt stick-slip sliding and dislocation of grains in the shear zone. The intensity of the noise and the magnitude of the peaks on the plot seem to be a function of the grain size, relative density, and presence or absence of fine-grained material in the matrix.

In fine-grained sediments, the traces were extremely smooth, with variations in point-load usually attributed to variations in density and to bedding planes. The coarse sediments, particularly the gravels, became more obvious with extremely irregular point-loads. The variations ranged from traces with a slight "sawtooth" characteristic to traces with great fluctuations and spikes. The increase in the irregularity appeared to be related to an increase in pebble size as well as density of the gravel. Fairly smooth traces were observed in sandy sediments, but as noted previously, point loads were usually higher than those associated with silt and clay.

The expanded view of a portion of the point resistance profile from probe site PH-10 (Fig. 4) demonstrates these influences. The most irregular parts of the plot (and severest noise and shaking) corresponded to clean, relatively

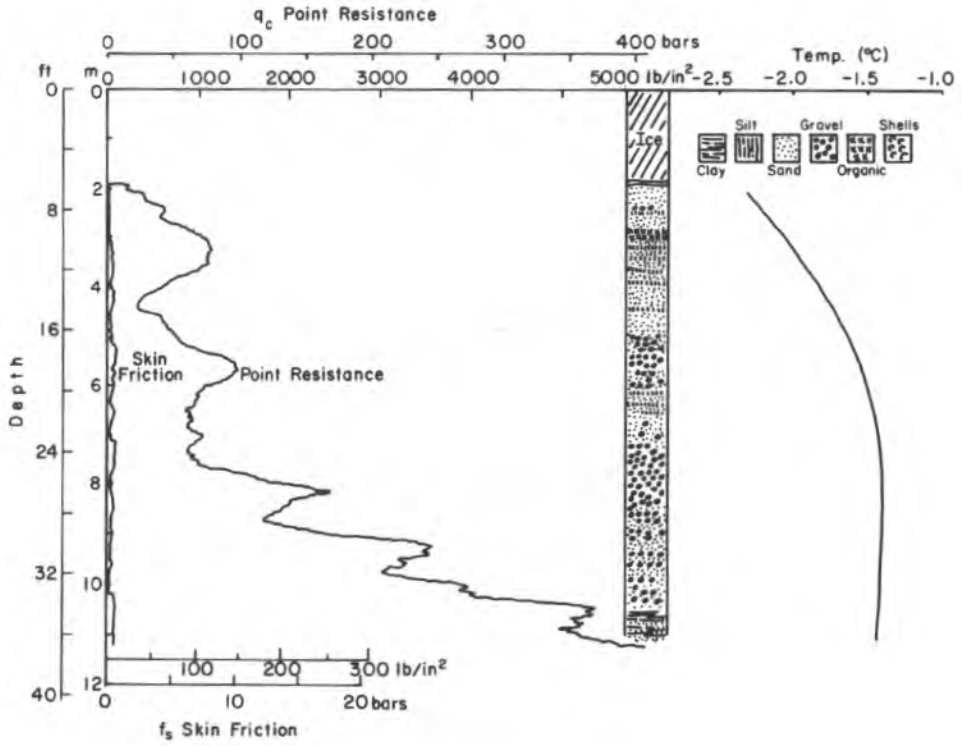

Figure 11. Comparison of point resistance and skin friction at probe PH-10 with geologic profile at drill site PB-6A.

coarse-gravel layers. As grain size decreased and silt became intermixed, the intensity of the noise tended to diminish. In fine-grained materials there was no audible noise. The saw-tooth character of the total load plots was lost during digitization (due to the coarseness of the digitization) and subsequent scale reduction. Thus, this information was obtained directly from the original plots produced on the X-YY recorder.

In addition to the grain size information available from the point-load traces, it appears that point-load response to change in penetration rate provides some information on distribution of frozen (ice-bonded) sediments. This results from the strong dependence of strength on loading rate in frozen soils, a dependence well documented by many investigators [see, for instance, Scott (1969) and Ladanyi (1976)]. The average penetration rate used in all tests was about 30 cm/min (12 in./min). This rate could be varied by adjusting the hydraulic pump. It was noticed that small variations in the penetration rate had no effect on the point load in either fine-grained or coarse-grained materials. In frozen materials, however, increasing the penetration rate caused a significant increase in point load. An example of this effect is shown in the expanded portion of the point load profile from probe site PH-16 (Fig. 12). A slight increase in penetration rate resulted in a corresponding increase in point load, and a decrease in point load occurred with a reduction in penetration rate.

In general, it was extremely difficult to penetrate frozen sand and impossible to penetrate frozen gravel. Penetration of a frozen sand was possible using a small (4.6-cm or $1^{13}/_{16}$-in.-diam) point pushed at a very low penetration rate. Point resistance was on the order of 690 bars (10,000 lb/in.^{2}). In some cases frozen fine-grained material could be penetrated with the large point driven at the standard rate with a point resistance on the order of 170 bars (2500 lb/in.^{2}). However, since no samples of these materials were collected at the probe sites where this occurred, the specific material characteristics are unknown.

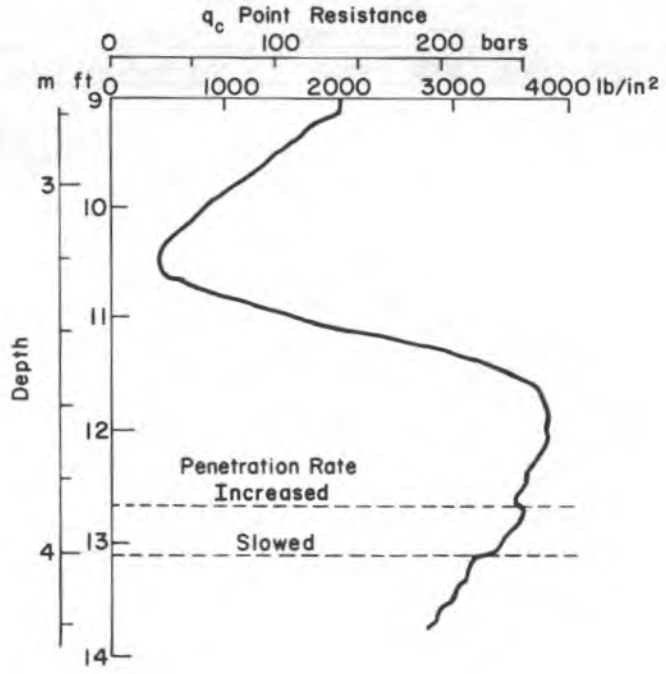

Figure 12. Expanded portion of site PH-16 point resistance.

Lithologic and temperature profiles

Once correlations had been established between point resistance data and the core logs from the five common sites, the additional data, including the thermal profiles, were examined in an attempt to determine the variations in bottom conditions along the three major survey lines (1, 2 and 3). Using the established correlations, all point resistance data were examined and converted to material logs. This was done independently by two individuals with extremely good agreement between the two interpretations. The resulting material logs for the three survey lines are shown in Figures 13 through 15.

Line 1 (see Fig. 6) ran generally normal to the coast and crossed an offshore bar. The end south of the line was in a more restricted lagoonal-type setting, while the end north of the bar was in a more open marine setting. The most noticeable feature of this line is the shallow bar occurring in the center of the profile where, seasonally, sea ice freezes back to the bed. It is in this zone that frozen materials were encountered at the bed surface. Seasonally frozen bed sediments were penetrated in holes PH-4, 5 and 9 where the bed depths were 1.5, 0.9, and 1.3 m (4.9, 3.0, and 4.3 ft), respectively, and possibly in a thin frozen layer at the bed in PH-8 where the bed depth was 1.6 m (5.3 ft).

There was good evidence that the deeper sediments in PH-5, the shallowest site examined, were frozen. As shown in Figure 13 and in the point resistance data in Appendix B, refusal was reached at a much shallower depth (7.5 m or 24.5 ft) than in holes PH-4 and PH-9 on either side of PH-5. This layer at which refusal was reached was exceedingly hard, as evidenced by the point resistance plot for test PH-5A shown in Figure 16. A small 4.6-cm- ($1^{13}/_{16}$-in.)-diameter point was fabricated and driven using the AW drill rod without the casing in an attempt to increase the penetration depth of test PH-5. An increase in depth of only 1.4 m (4.5 ft) was achieved using the small point, even though the point load was probably increased to approximately 650 bars (9500 lb/in.^{2}). The exact point load could not be determined because the side friction acted directly on the drill rod; thus only total load was plotted as a function of depth. Even though the

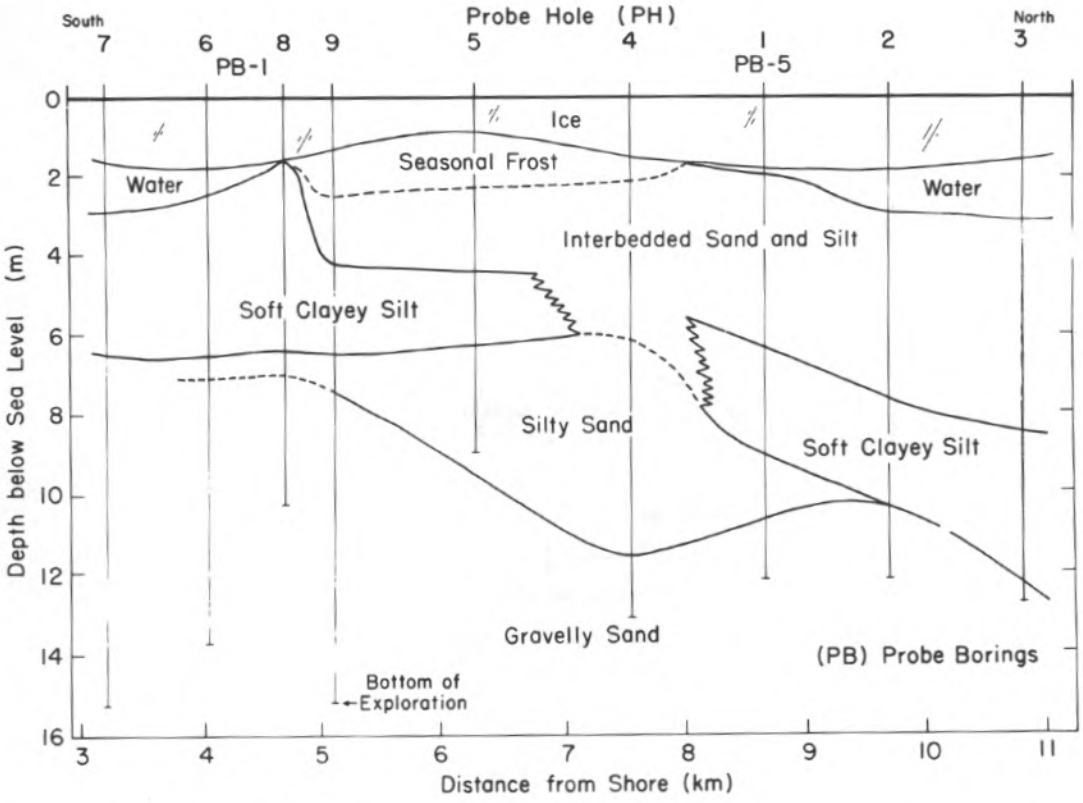

Figure 13. Stratigraphic profile interpreted from probe data along line 1. (1 m = 3.28 ft; 1 km = 0.62 mile)

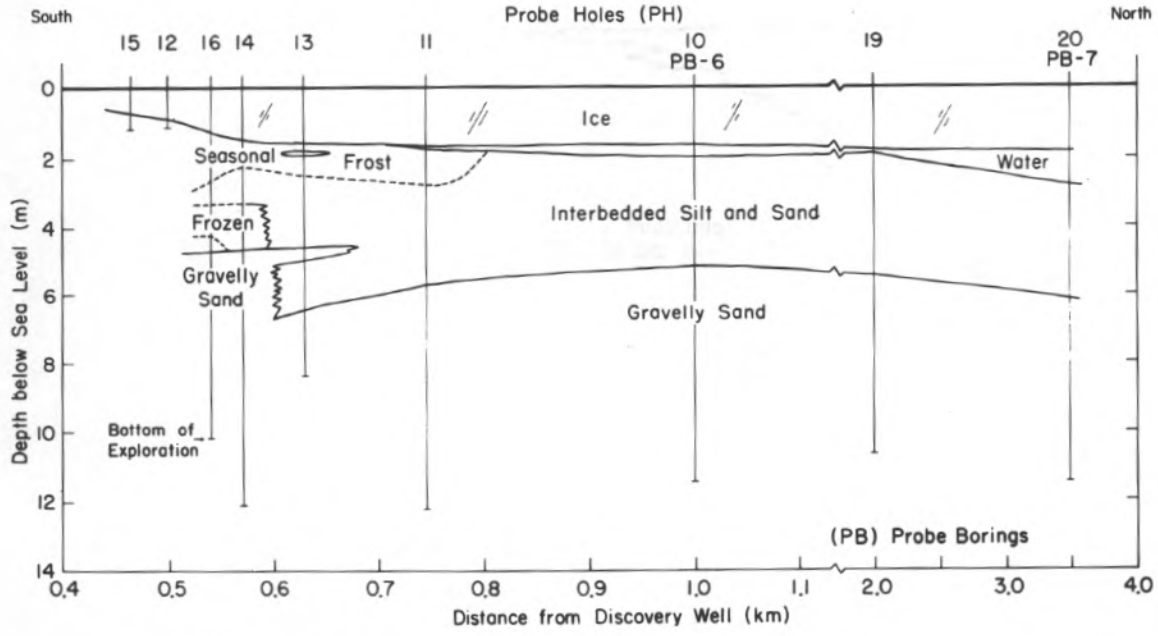

Figure 14. Stratigraphic profile interpreted from probe data along line 2. (1 m = 3.28 ft; 1 km = 0.62 mile)

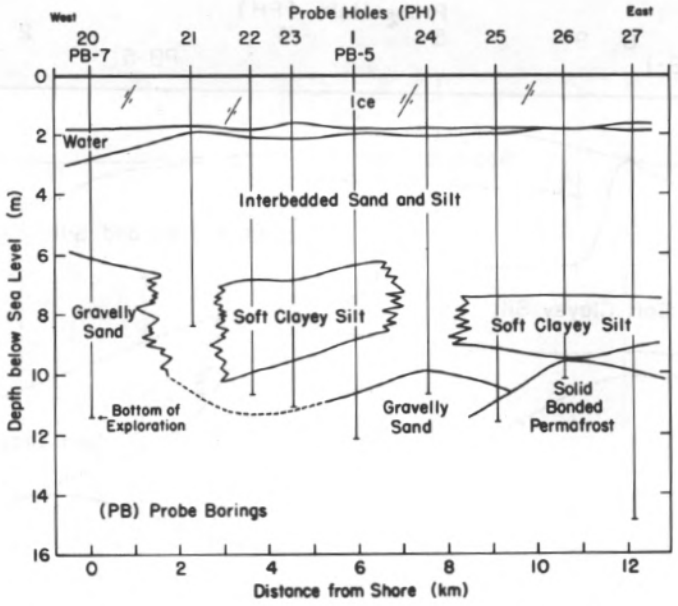

Figure 15. Stratigraphic profile interpreted from probe data along line 3. (1 m = 3.28 ft; 1 km = 0.62 mile)

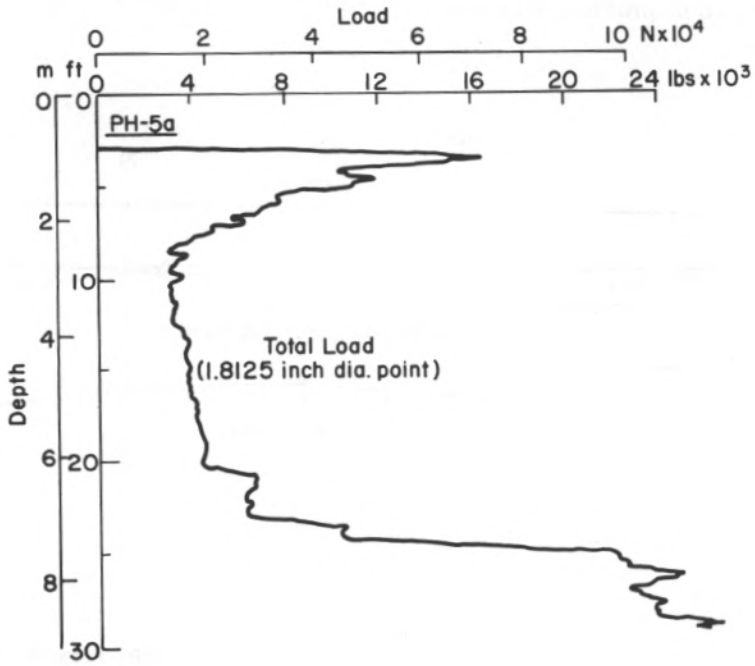

Figure 16. Results of special test at site PH-5a with small point.

point load was doubled, only a small increase in penetration depth was achieved, which was still much less than at the immediately adjacent sites where the larger point was used.

Additional evidence of ice-bonded sediments, at least in the upper part of the section, can be inferred from the thermal profiles shown in Figure 7. The sediment temperatures at the three probe sites in the shallow water over the center portion of the bar (PH-4, 5 and 9) were significantly lower, both near the surface and at depth, than the sediment temperatures landward or seaward of the bar. Although the freezing temperature of the water in these sediments is unknown, chemistry data from nearby boreholes indicate that the freezing point was most likely in the range of −1.75 to −3.55°C (28.85 to 25.61°F) (Page and Iskandar 1978). If the freezing points of the water in the upper part of these sediments fell within this range, then it is almost certain that they were ice bonded.

Although the temperatures at depth at sites PH-4 and 9 are lower than the freezing point of normal sea water [−1.75°C (28.85°F)], these deeper sediments probably remain unfrozen because of the exclusion of salts during freezing from the sediments above, which results in higher salinities and lower freezing points in the deeper sediments. However, the temperature (−3.25°C) at the deepest point penetrated at site PH-5 is much colder than at the adjacent sites PH-4 and 9 (see Fig. 7). Because of this and because penetration refusal was reached at a depth much shallower than at any of the other sites along this line, it is possible that ice-bonded sediments were encountered. This is uncertain because at this depth it also appears that dense gravelly sands are encountered.

It is probable that the ice-bonded sediments found at shallow depths are formed seasonally while the ice-bonded sediments at greater depths are frozen year-round; i.e., they are bonded permafrost.

According to the material profile interpretations of Figure 13, the probe sites landward of the shoal have lithologic sections that are different from those to the seaward side of the bar. A fine-grained section occurs from the surface down to the coarse-grained sediment in PH-8, 6 and 7, an indication of very quiescent depositional conditions typical of a lagoonal setting. These fine-grained sediments are also found under the bar complex (PH-5 and 9) overlying the deeper coarse sediment, although in this case they are capped with sandy sediments.

This coarser sandy and silty material is probably discharged from the Sagavanirktok River forming the shoal area. Seaward from the bar or shoal area, the surface sand and silt unit increases slightly in thickness and caps a fine unit (clay-silty clay). These clay to silt- sediments below the coarse sediment cap must reflect deeper marine deposition or deposition in a lagoon similar to the sediments found near the bed shoreward of the shoal.

The second major survey line, running seaward adjacent to the ARCO dock (see Fig. 6), was an uninterrupted transition from near shore to water depths approaching 3 m. One obvious feature of this survey (see the penetration resistance data in App. B and the material profiles in Fig. 14) is that penetration of the near-shore seasonally frozen coarse-grained sediments was very limited. At the two most shoreward sites, PH-12 and 15, having the coldest bed temperatures, the frozen sand could not be penetrated. Seaward from these sites, the frozen bed could be penetrated, with penetration resistance decreasing with increasing water depth and distance from shore. The absence of seasonally frozen bed sediments detectable by this probe corresponded closely to bed depths where some water existed between the ice and the bed. Frozen sediments were encountered in PH-12, 13, 14, 15 and 16, with possibly some frozen bed sediments in PH-11.

A distinctive profile was noted at PH-16 (see Fig. B16, App. B), where point resistance, penetration characteristics, and thermal data are suggestive of alternate layers of frozen and thawed sediment. This may be explained by the fact that salt exclusion from downward freezing can cause zones rich in unfrozen brine followed by frozen zones of low pore water salinity. The thickness and ultimate layering characteristics are strongly dependent on sediment distribution, thermal gradients, freezing rates, and original pore water chemistry. Layering in the seasonally frozen sediment may also have existed in both PH-13 and 14, though the penetration records are not as conclusive as those of PH-16.

Frozen sediments also appear to exist in the base of PH-16. Based on the probe response data, and thermal probe records that indicate temperatures as low as −2.5°C (27.5°F) in this zone, it is likely that these are perennially frozen sediments.

Line 3, which was approximately normal to the previous lines, shows several interesting features. This profile (see Fig. 15), unlike the

other sections, was made at a uniform water depth and no seasonal freezing in the bed was noted. However, there were indications that deeper frozen (ice-bonded) sediments were present on the east end of the line toward the bottom of PH-26 and 27 and possibly at the bottom of PH-25. The supporting evidence for frozen sediment near the base of PH-27 is quite strong. The shape of the point resistance profile indicates fine-grained material, but the point resistance was much higher than normal for fine-grained materials in this area. In addition, the PH-27 thermal profile in Figure 9 shows a temperature of −3.5°C (25.7°F) at the bottom of the hole, which is well below the freezing point of normal sea water; however, chemistry data needed to establish the actual freezing point were not available at this site.

The thermal data along this line are notable since it would generally be assumed that the thermal environment should have been fairly uniform throughout the line. However, the thermal profiles show a marked deviation from the assumed uniformity. The central and western holes all have thermal gradients that cluster in the range of those usually found in areas that do not freeze back to the bed. However, as the eastern end of the line was approached, progressively colder temperatures were encountered. It is not certain what historical differences may have existed along this line. It was suggested that this eastern, colder zone may reflect an area in which recent erosion has removed some surface sediments which have in recent times been in contact with the sea ice during the winter.

The geology along this line appears to be quite consistent. The near-surface sections in all holes consist of interbedded sand and silt. These sediments generally grade into fine clay-rich sediment along most of the line, before making the transition into the coarse-grained material.

Casing penetration resistance

While casing load profiles were obtained from most tests, quantitative analysis of these data is difficult because of the design of the apparatus. Most of the casing load data came from mea surements on the casing assembly shown in Figure 3. The 6.35-cm (2½-in.)-diameter by 15.24-cm- (6-in.)-long casing shoe welded to the 5.72-cm- (2¼-in.)-diameter casing was pressed into the sea floor behind the shrouded point. The casing resistance equaled the sum of the frictional resistance acting on the casing shoe plus any component of side friction resulting from collapse or rebound of the hole around the casing above the point and shoe assembly. It is impossible to quantitatively separate these two components. Generally, total casing load was quite low, usually less than 8.9 kN (2000 lb). If an 8.9 kN (2000 lb) load was borne entirely as shear on the casing shoe, shear stress would average a relatively high 2.9 bars (42 lb/in.^{2}) over the shoe surface. However, casing load tended to increase with increasing depth of penetration, probably indicating that a portion of the high casing load resulted from soil acting on the casing.

At site PH-3, a modified point assembly was tested in which an unshrouded 5.72-cm- (2¼-in.)-diameter point was pushed ahead of the 5.72-cm- (2¼-in.)-diameter casing without a casing shoe. Thus, the hole made by the point was exactly the diameter of the casing, making this test analogous to that of a foundation pile. As shown in Figure B3 (App. B), a significant portion of the total load on the string was needed to advance the casing. Even though a majority of the 9.75-m (32-ft) penetration was through fine-grained material having almost no point resistance, the casing resistance built steadily to almost 40 kN (9000 lb) before the point reached refusal in a gravel layer. The average shear resistance over the entire casing length was about 0.23 bars (3⅓ lb/in.^{2}). Even though the soil profiles at most of the test sites seem ideally suited for end-bearing piles founded on dense gravels, this test suggests that significant bearing capacity at shallower depths could be generated by the side friction shear component as well.

APPLICATIONS

There has been an extensive effort, mainly in Europe, to develop both static penetrometer equipment and standardized engineering application procedures using the data from these tests. Sanglerat (1972) and the European Symposium on Penetration Testing (1974) have excellent summaries on the varied equipment and procedures in use throughout the world. Sanglerat summarizes this work in a set of recommendations for making direct application of point resistance data in the design of both

shallow and deep foundations. Because the static penetration test is not well known in this country, and because it demonstrates the potential utility of the data gathered in the Prudhoe Bay area, these recommendations are briefly summarized here.

Shallow foundations

The allowable bearing pressure in *cohesionless* soils (which constitute the bulk of the shallow sediments in the Prudhoe Bay region of the Beaufort Sea) for conventional spread footing ½ m (½ yd) in width and at an equivalent depth may be taken as $^1/_{10}$ the point resistance:

$$q_{ad} = q_c/10 \quad (1)$$

where q_{ad} is the allowable bearing stress and q_c the point resistance. Generally the allowable stress is taken as about ⅓ of the ultimate strength.

In *cohesive* soils, the undrained shear strength c_u (apparent cohesion) is somewhat dependent on the type of penetrometer. For normally consolidated sandy clay:

$$q_c/10 < c_u < q_c/20 \quad (2)$$

and the failure load q_{ul} can be calculated from:

$$q_{ul} = 5.7\, c_u \quad (3)$$

for long footings and

$$q_{ul} = 6.8\, c_u \quad (4)$$

for square or circular footings. Again, Sanglerat recommends that the allowable bearing stress be taken as ⅓ of the failure load.

Estimates of settlements and differential settlements of shallow footings in cohesive and cohesionless soils can be made from penetrometer data. Sanglerat (1972) summarizes several techniques for predicting settlement; however, these are beyond the scope of this report. He recommends use of point resistance data to classify soils broadly into two categories. In soils with q_c's greater than 12 bars, settlements of shallow footings embedded 1 to 2 m (1 to 2 yd) are generally negligible. In soils with q_c's of less than 12 bars, significant total or differential settlements may occur. In these cases, settlement analyses using point resistance data or other techniques must be performed.

Deep foundations

According to Sanglerat, static penetrometer point resistance can be used directly to give values of allowable bearing pressure for use in design of end bearing piles. Allowable bearing pressure is given by:

$$q_{ad} = q_{ul}/F \quad (5)$$

where F is the safety factor. For a pile embedded a minimum of 8 pile diameters into a thick, homogeneous bearing layer, the failure load q_{ul} can be assumed equal to the point resistance q_c with a safety factor of 2 chosen for values of point resistance less than 100 bars. For these conditions, allowable bearing is given by:

$$q_{ad} = q_c/2 \quad (6)$$

For point resistances of more than 100 bars, such as were encountered in the deeper gravelly sands, the safety factor should be increased to account for excessive loads on the concrete filling of the pile, which Sanglerat feels should not exceed 50 bars. He also cautions that for values of point resistance below 80 bars, where end bearing is in a sand layer below the water table, liquefaction may result from subsequent driving, resulting in loss of end bearing. In such cases, he recommends that full-scale pile load tests be performed, particularly when values of q_c are less than 50 to 60 bars.

In homogeneous clay layers, Sanglerat recommends that the safety factor in eq 6 be raised to 3.

For bearing layers that are not homogeneous, Sanglerat recommends the method used by Fugro, where ultimate bearing capacity is given by:

$$q_{ul} = \frac{\frac{q_{c0}+q_{c1}}{2} + q_{c2}}{2} \quad (7)$$

where q_{c0} is the average penetration resistance over a depth of two pile diameters beneath the pile tip, q_{c1} is the minimum penetration resistance over the same two diameter interval, and q_{c2} is the average minimum point resistance over a height of 8 pile diameters above the tip. The allowable bearing pressure is given by eq 5 with a safety factor of 2 for cylindrical piles and 2.5 for piles with enlarged bases.

Sanglerat cautions that a bearing layer must extend *well below* the potential failure surfaces

beneath the pile tip. This requires that the vertical extent of potential bearing layers be determined either by penetrometer data or by drilling if the penetration resistance is too high.

Sanglerat does not recommend the use of penetrometer data for the design of friction piles; rather he recommends the use of full-scale in-situ pile load tests to determine both bearing capacities and settlement characteristics.

Foundations in permafrost

In instances where offshore structures bear on bonded permafrost, foundation design may be considerably more complicated. While bonded permafrost is generally a strong material, excessive settlement can occur if heat transfer through the foundation melts the interstitial ice in the permafrost. In addition, even if no melting occurs, differential creep settlements may be a problem in time, especially in fine-grained permafrost with high salt and ice contents. Thus, options open to the foundation designer tend to be limited by the material.

A coarse-grained, thaw-stable permafrost would present no additional problems to the designer, while a fine-grained, ice-rich permafrost would be unstable if allowed to thaw and in the frozen state might be subject to excessive creep settlement. Design of foundations in such material is covered in the literature, e.g., Sanger (1969); but there will certainly be problems peculiar to the subsea setting, such as marginal temperatures, presence of salt, lateral loads of ice, etc., which will mean additional complications to the already difficult design problems.

Based on the penetrometer results, some general conclusions may be drawn regarding offshore foundation types in the Prudhoe area. The deep unfrozen sandy gravel which is prominent along all survey lines appears to be an excellent bearing layer for end bearing pile or caisson foundations. The depth to the top of the layer is not excessive, generally between 6 and 12 m below sea level, and the point resistance increases rapidly with depth in this layer to values of hundreds of bars.

In some areas it may be possible to use shallow foundations based in the unfrozen interbedded sand and silt. This application would require great care, however, as excess settlements and differential settlements could occur due to the interbedding and/or underlying soft clay layers. For instance, in point PH-3, the interbedded sand and silt to a depth of 7 m would be sufficient support for shallow foundations for many applications; but the very soft, silty clay layer from 7 to 12 m would likely preclude the use of shallow foundations for any substantial structure at this location.

CORRELATIONS WITH LABORATORY TESTS

Staged triaxial compression tests have been run on a number of core samples from several of the drilling sites. Stress-strain data from the three tests at PB-5, and the single test at PB-6 (corresponding to probe sites PH-1 and 10 respectively) are shown in Figure 17. Confining pressure was held constant at the estimated in-situ pressure throughout the initial portion of each test. As each sample approached failure, the confining presure was increased. On the two nonplastic silts from PB-5 and on the silty sand from PB-6, this produced an increase in shear stress due to the frictional behavior of these materials. The confining pressure increase had no effect on the stress-strain curve of the plastic silt from PB-5, indicating that the coefficient of internal friction ϕ was zero for this material. The silty sand sample from PB-6 had a stress-strain curve that was distinctively different from those for the silt samples of PB-5. A well defined failure occurred at less than half the strain associated with failure in the silts. Such behavior is characteristic of the material property differences between the two materials.

Comparisons between the peak shear strengths from the four tests and the point resistance profiles from the corresponding probe holes are shown in Figure 18. There appear to be a considerable number of inconsistencies in these correlations. The point resistance values for the two deeper silt samples in PH-1 are of the same relative magnitude as the shear strengths (both very low). However, the point resistance values for the shallow nonplastic silt and for the silty sand are both approximately two orders of magnitude higher than the laboratory shear strengths.

There are several possible explanations for these discrepancies. First, the laboratory samples, as frequently is the case, may not have

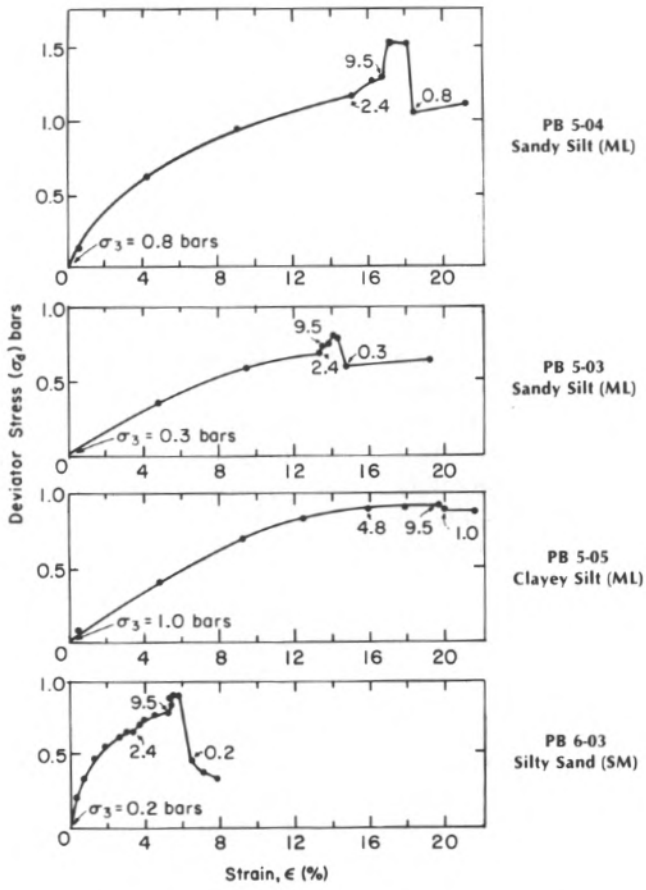

Figure 17. Results of staged triaxial tests for four test samples obtained from sites PB-5 and PB-6. (1 bar = 14.5 psi)

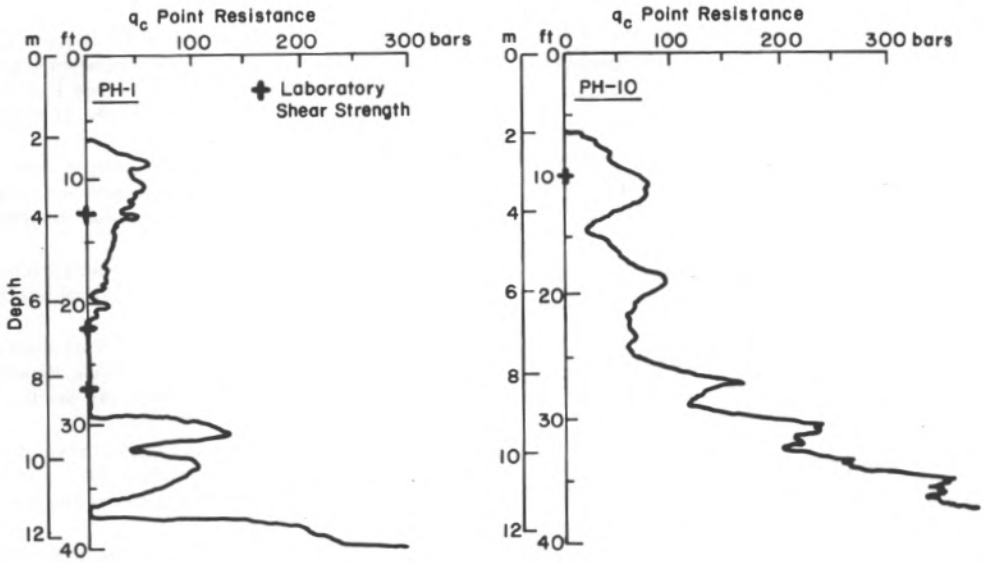

Figure 18. Comparison of triaxial test results with point resistance data at sites PH-1 and PH-10.

been respresentative of the bulk of the material in the vicinity of the samples. In selecting samples, the "best" pieces of core were chosen because they were the only pieces satisfactory for testing. In both cases, these were not representative of the bulk of the material in a given core section, but were taken from fine-grained silt or silt lenses within a coarser sand section. Another possible explanation may be that minor local variations over the 100- to 200-ft distances between the boreholes and the probe holes were such that details of the material layering between the two may not exactly correspond. In either case, the lack of consistent correlation between the field and laboratory data once again emphasizes the difficulty of making in-situ characterizations using extrapolations of laboratory data.

CONCLUSIONS

The static cone penetrometer provided an effective means of rapidly acquiring information on engineering properties of sediments in an arctic marine environment. When correlated with information obtained from a few drill holes the penetration resistance data permitted construction of geologic profiles. The penetrometer was also a useful tool for determining the occurrence of subsea permafrost because temperature profiles could be readily obtained. (By classical definition permafrost is that material where the temperature remains below 0°C for several years or more.) However, because of a lack of information on salt concentrations in the pore water of the sediments, freezing temperatures were unknown or at best could only be estimated based on a few drill hole determinations. The temperature data, though, when augmented by penetration resistance characteristics, did allow the determination of ice-bonded zones.

In the Prudhoe Bay region of the Beaufort Sea, it appears that fine-grained sediments overlie coarser sand and gravels at most of the sites investigated. The thicknesses and penetration resistances of the different sediment types vary considerably over the area. Seasonally frozen sediments were found to occur in shallow waters where the sea ice froze to or near the seabed. Perennially frozen sediments were observed in the deeper sands and gravels at several sites. High penetration resistances were characteristic of all sites where frozen materials were encountered. Although it appears that the occurrence of shallow, ice-bonded material can be expected in very shallow water, the occurrence of deeper, perennially frozen sediments is less predictable.

The depth of penetration was limited only by the load capability of the apparatus. In very shallow waters where cold, seasonally ice-bonded coarse-grained sediments were encountered, little or no penetration was possible. In deeper waters where the sea ice was not in intimate contact with the seabed, penetration was usually limited by either perennially frozen sediments or by very dense and stiff gravels. Ten to twelve meters of sediment was commonly penetrated. Buckling of the unsupported penetrometer column can be a problem when water depths exceed a few meters.

Coarse-grained, non-ice-bonded permafrost would present no particular problems to the designer of foundations for offshore structures. However, because of the uncertainties related to the occurrence of ice-bonded sediments, and because of the extreme variability in material types and penetration resistance observed, it is concluded that foundation design in this region is very much related to the specific site.

SELECTED BIBLIOGRAPHY

Chamberlain, E.J., P.V. Sellmann, S.E. Blouin, D.M. Hopkins and R.I. Lewellen (1978) Engineering properties of subsea permafrost in the Prudhoe Bay region of the Beaufort Sea. Proceedings of the Third International Conference on Permafrost.

Heijnen, W.J. (1974) Penetrating testing in Netherlands. Proceedings of European Symposium on Penetration Testing, Vol. I, *National Swedish Building Research*, Stockholm, Sweden.

Ladanyi, B. (1976) Use of the static penetration test in frozen soils. *Canadian Geotechnical Journal*, vol. 13, no. 2, p. 95-110.

Osterkamp, T.E. and W.D. Harrison (1976) Subsea permafrost at Prudhoe Bay, Alaska—Drilling Report. Univ. of Alaska, Scientific Rpt. UAF R-245, Sea Grant Rpt. No. 76-5.

Page, F.W. and I.K. Iskandar (1978) Geochemistry of subsea permafrost at Prudhoe Bay, Alaska. Cold Regions Research and Engineering Laboratory Special Report 78-14. AD A060434.

Sanger, F.J. (1969) Foundations of structures in cold regions. CRREL Cold Regions Science and Engineering Monograph III-C4. AD 694371.

Sanglerat, G. (1972) The penetrometer and soil exploration. New York: Elsevier Publishing Company.

Scott, R.F. (1969) The freezing process and mechanics of frozen ground. CRREL Cold Regions Science and Engineering Monograph II-D1. AD 697136.

Sellmann, P.V., E.J. Chamberlain, H.T. Ueda, S.E. Blouin D.E. Garfield and R.I. Lewellen (1977) CRREL-USGS Subsea permafrost program, Beaufort Sea, Alaska: Operational Report. CRREL Special Report 77-41. AD A048985.

APPENDIX A: DESCRIPTION OF PENETROMETER AND TEST PROCEDURES

TEST APPARATUS

Based upon the 1976 field experience and a review of current literature on penetrometers, two separate testing methods were planned: the first, a so-called "static" test in which the point and casing assembly are advanced at a relatively slow rate (less than 2 cm/s) (0.8 in./s); the second, a dynamic test in which repetitive blows from a heavy weight provide the driving force for the drill rod and casing. Requirements placed on the total system were that: a) it be easily transportable over snow-covered ice; b) the unit be as compact as possible for shipping purposes; and c) the unit have a power source for remote operation. Since drill string buckling was a problem in the 1976 tests, heavier AW casing and drill rod were selected to push the point because of their greater column stability.

STATIC APPARATUS

Original design requirements of the static penetration system were that: a) it be capable of exerting a 133-kN (30,000 lb) force on the drill rod and casing; b) it be capable of attaining a maximum penetration rate of 2.0 cm/s (47.2 in./min.); c) the load must be capable of being applied to the drill rod or casing independently or to both drill rod and casing simultaneously; and d) some means be provided to measure the penetration resistance as a function of probe depth.

The probe was designed around a standard 60° cone. It was similar in design to the Dutch mantle cone. A 7.0-cm- (2¾-in.)-diameter cone was machined to 6.35-cm (2½-in.) diameter, and pinned to the drill rod so the point was recoverable. Since the magnitude of the frictional forces between the casing and hole wall was unknown, it was decided to provide for 15.2 cm (6 in.) of relative axial movement between the drill rod and casing, allowing independent movement of the casing or drill rod. This was accomplished by attaching a stainless steel shroud to the point assembly. The inner diameter of this sleeve was slightly larger than the casing outside diameter, while the sleeve outside diameter was tapered to reduce the influence of sidewall friction effects on it. Above this stainless steel sleeve, a 6.35-cm- (2½-in.)-diameter sleeve 15.2 cm (6 in.) long was welded to the casing. The idea was that the majority of casing side wall friction forces would be concentrated at this enlarged section, allowing some distinction between frictional forces in various materials. The complete point assembly is shown schematically in Figure 3. A photograph of the point is shown in Figure A1.

It was decided that a self-contained test sled that could be towed to the test sites with a crawler tractor would be desirable. Rather than setting anchors in the ice to provide the reaction forces as had been done the previous year, the towing tractor was backed onto the test sled, thus providing the necessary vertical reaction force. Photos of the test sled being towed and with the tractor on board are shown in Figures A2 and A3, respectively.

The building frame was fabricated from structural angle, channel, and I-beams to withstand the 133-kN (30,000-lb) maximum applied vertical force. The sled skis were fabricated from a 45.7-cm (18-in.) structural channel and extended about 4 m (13 ft) beyond the rear of the building. The distance between the skis was such that the majority of crawler tractors in the weight range required could be accommodated. Two 20.3-cm (8-in.) wide-flange I-beams spanned the width of the building and provided a reaction frame for the main hydraulic ram, as well as a trolley track for a traveling hoist unit. A skin of 1.3-cm (½-in.) plywood covered the building. A photo of the test sled before application of the plywood skin is shown in Figure A4. A door was provided in the front of the building and a double-pane acrylic window was installed on the side of the building facing the front of the sled. The diesel generator, hydraulic power supply, and fuel supply were contained in a module, shown in Figure A5, attached to the side of the building towards the front of the sled. Waste heat from the generator and hydraulic unit provided ample heat for maintaining the uninsulated building at above freezing temperatures even with ambient temperatures at −40°C (−40°F).

Figure A1. Penetrometer casing and point.

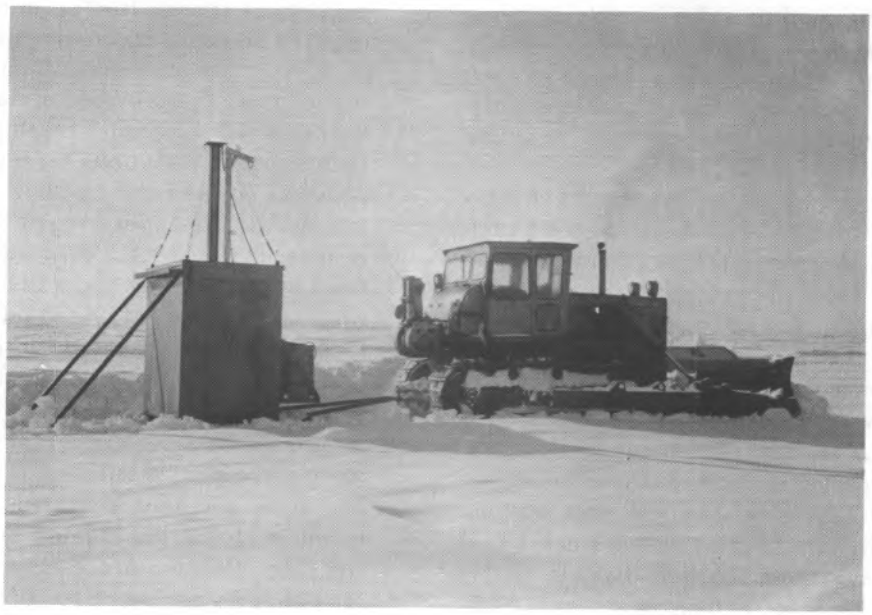

Figure A2. Tractor towing penetrometer sled.

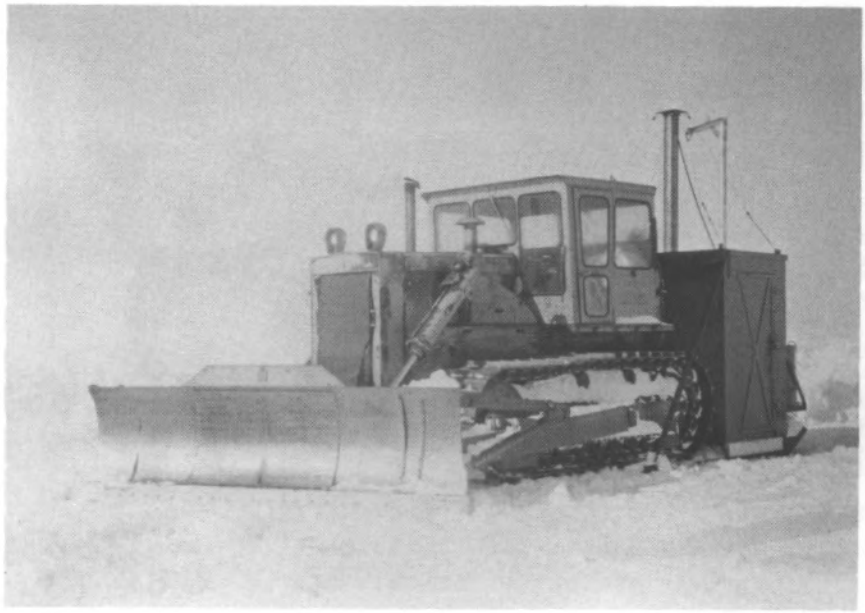

Figure A3. Tractor on sled runners to provide reaction force.

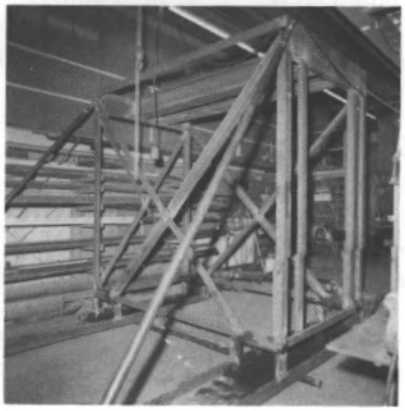

Figure A4. Interior of sled building before application of plywood skin.

Figure A5. Diesel generator attached to side of the sled building.

The hydraulic system provided power for driving and extracting the penetrometer. The power supply consisted of a 3-hp electric motor driving a pressure-compensated, variable-volume vane-type pump, all mounted atop a 37.85-liter (10-gal.) hydraulic reservoir. The pump was capable of pumping 15.1 liter/min. (4 gal./min.) at 69 bars (1000 lb/in.^{2}) or 6.8 liter/min. (1.8 gal./min.) at 103 bars (1500 lb/in.^{2}). The double-acting hydraulic ram, bolted to the I-beams on the top of the building, had a 12.7-cm (5-in.) bore and a 183-cm (72-in.) stroke. The cylinder stroke would accommodate standard 152-cm (60-in.) lengths of drill rod and casing. An oversized 6.35-cm- (2½-in.)-diameter piston rod was selected to provide greater column stability when driving the penetrometer. The ram was capable of driving at 2.0 cm/s (47.2 in./min.) with a driving force of approximately 89 kN (20,000 lb). This capability was reduced to a rage of 0.9 cm/s (21.3 in./min.) with a driving force of 133 kN (30,000 lb). The pressure compensated pump applied essentially a constant power input to the system. A schematic diagram of the complete hydraulic system, including the dynamic system described later, is shown in Figure A6.

The force measuring system was designed to separate the point driving force from the friction force of the casing against the hole wall. A diagram of this arrangement is shown in Figure A7. The lower hollow load cell measured only casing forces. The total of casing force plus point load was measured by the upper load cell. Outputs from both load cells were amplified and continuously recorded on an X-YY chart recorder as a function of penetration depth. Penetration depth was measured in 152-cm (60-in.) increments with a cable-actuated potentiometer. Thus, a continuous record of penetration force versus depth of penetration was obtained.

DYNAMIC APPARATUS

A dynamic test apparatus was also designed and built to provide a means for further driving the penetrometer after the static system could no longer provide the necessary force. The apparatus consisted essentially of a large, 590-kg (1300-lb) cylindrical steel hammer dropped 30.5 cm (12 in.) onto an anvil. A guide tube was provided to stabilize the large hammer. The hammer was raised with a pair of hydraulic cylinders. A pilot-operated hydraulic pump valve was set to release when the hydraulic pressure rose to a set point somewhat above the pressure required to raise the hammer. The higher pressure was obtained when the hammer contacted a mechanical stop on the guide tube. A hydraulic time delay circuit was designed to hold the dump

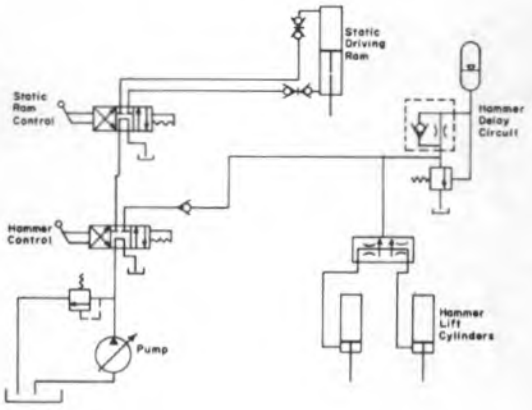

Figure A6. Schematic of hydraulic loading system.

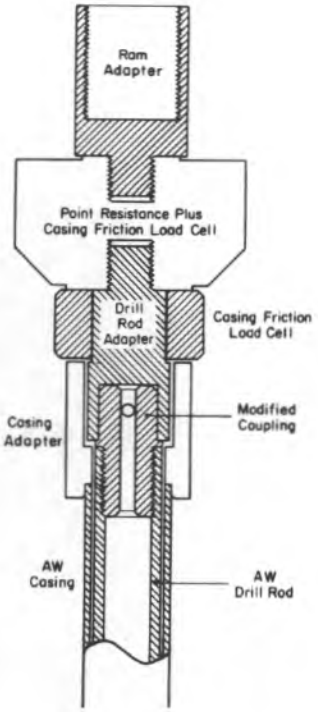

Figure A7. Diagram of force measuring system.

valve open and allow the hammer to free-fall onto the anvil. The guide tube was rigidly fastened to the anvil and extended through a centrally located guide hole in the hammer. Two back-to-back channels rigidly attached to the top of the guide tube provided a means for attaching the hydraulic lift cylinders. A schematic view of the hydraulic system is shown in Figure A6 and the hammer is shown in Figure A8.

A maximum repetition rate of 30 blows/min. allowed manual counting of the number of blows for a given depth of penetration. The dynamic test apparatus was maneuvered into position using the hoist and trolley system mentioned previously. It was then suspended from the piston rod of the static force apparatus, and was piloted onto the casing and drill rod through a hole in the anvil. When dynamic test apparatus was being operated, the static cylinder was placed in a "floating mode" so it would descend with the dynamic apparatus and exert little restraining force.

FIELD TESTS

Because the electric generator had not arrived prior to the scheduled shipment date, tests could not be performed on all of the equipment. Instead the majority of the equipment was shipped to Alaska by truck and the generator was shipped later by air. The equipment was assembled in a large building several miles from the test area. When all equipment was assembled and checked out, the test sled was removed from the building. Once the electric generator was started, it ran continuously during the entire 2-week test season, except for short periods while preventive maintenance was being performed. The crawler tractor also ran continuously during the test period.

A typical static test involved towing the test sled to a pre-selected test site (Fig. A2). In some cases, a road could be plowed as the sled was towed to a test site; however, if the snow was too

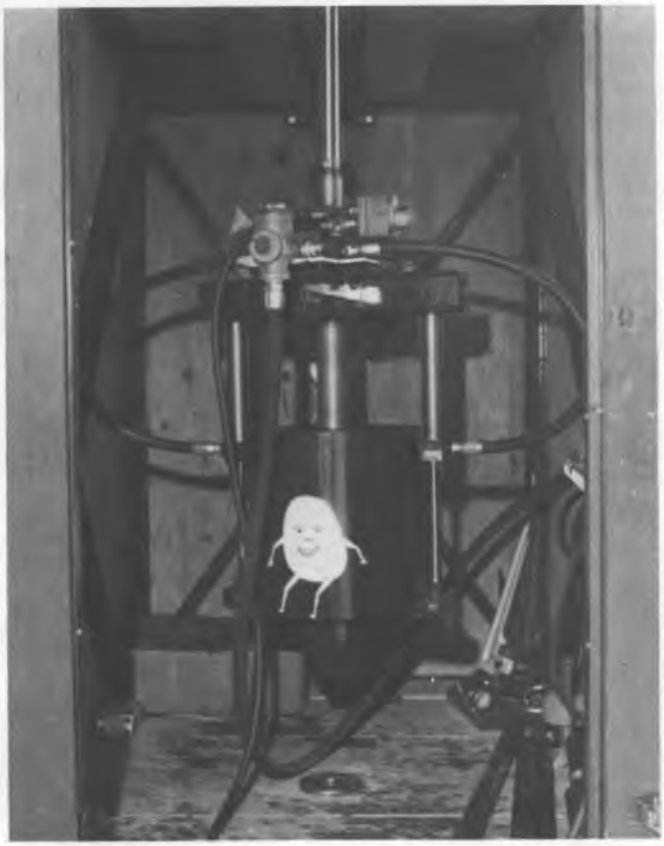

Figure A8. Drop hammer.

deep or too hard, the road plowing was accomplished on a separate trip with the tractor alone. The actual test site was cleared of snow by lowering the dozer blade to the ice surface, and making a single pass to clear an area slightly longer than the test sled. A 20.3-cm- (8-in.)-diameter hole was then augered through the ice using a gasoline engine-powered ice auger. The hole was centered with respect to the test sled using the towing hitch as a guide. This hole was drilled as close to vertical as possible to avoid alignment problems later. After the hole was drilled and cleaned, the sled was towed over the hole. One person, besides the tractor operator, was required to align the test sled. Correct alignment with the hole was accomplished by the second person visually sighting on a rod extended through the centrally located guide bushing in the building floor, and directing the tractor operator. After correct alignment was achieved, the tractor was unhitched from the sled and driven around to the rear of the sled. It was then carefully backed onto the runners until the tractor just contacted an I-beam attached to the side of the building (Fig. A9). This contact was required to aid the sled runners in resisting vertical building deflection during testing.

After the tractor was in position, all remaining work was performed inside the shelter. One person cleaned the penetrometer point and assembled this unit while the other person set up and performed a calibration test on the instrumentation. The instrumentation was set up such that a 25.4-cm (10-in.) vertical probe displacement produced 2.54 cm (1 in.) of horizontal pen displacement. Both load cell circuits were calibrated to produce a 2.54-cm (1-in.) of pen displacement for a 17.8-kN (4000-lb) load. After initial preparations, the penetrometer point was then lowered through the bronze bushing in the building floor, through the sea ice and water to the sea floor, and additional lengths of drill rod and casing were attached as necessary. Once in position, an adapter was

Figure A9. Detail of tractor on the sled.

screwed onto the upper end of the drill rod (Fig. A10). A second adapter was then placed on the casing, and the hydraulic ram lowered until contact was made with the drill string (Fig. A11). The ram was then raised slightly and all instrumentation channels zeroed (Fig. A12).

A measurement from the top of the drill rod to the building floor established the starting point, since the distance from the building floor to the ice surface was fixed. The ram was advanced to the end of its stroke, forcing the penetrometer point into the sediments. During ram retraction, the drill rod and casing adapters were removed and another length of drill rod and casing was readied for assembly. Ten lengths of drill rod and casing were stored inside the building, which was sufficient for the majority of tests performed. After the drill rod and casing were tightened, the adapters were again installed and another 1.52-m (5-ft) length was pushed into the sediments. The chart paper was changed every 3.0 m (10 ft) of penetration. This process was repeated until the penetration resistance was sufficiently high to prevent further penetration. A penetration resistance of 125 kN (28,000 lb) was considered "refusal." This limit was established because of the uncertainty on the amount of lateral support given to the column by the subsea sediments. The drill string did buckle on one occasion; however, quick action by the operator prevented any damage to the equipment or the drill string.

A complete static penetrometer test could be performed in about 3 hours. Since temperature profiles were also required, it was decided to perform one penetrometer test each morning, move to a new site, perform a second penetrometer test, and leave the drill string downhole to establish thermal equilibrium before temperature measurements were taken the following morning. Thus, in the 2-week test period 27 static penetrometer tests could be performed.

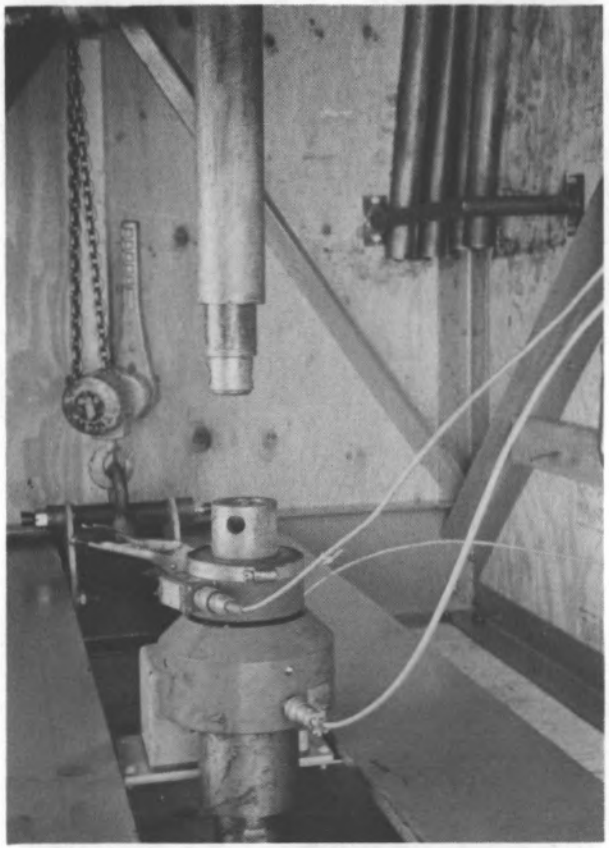

Figure A10. Detail before coupling ram and load cells to the drill rod.

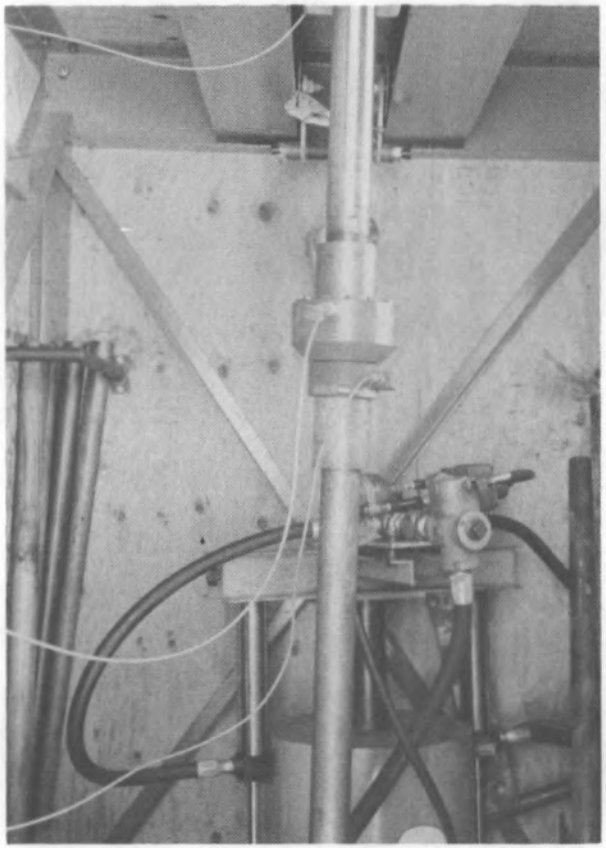

Figure A11. Detail after coupling ram and load cells to the drill rod.

Figure A12. Close-up of recording system.

Originally, it was planned to use the dynamic test apparatus to drive the penetrometer when refusal was reached with the static apparatus. The purpose in building the dynamic apparatus was to penetrate further into the hard materials to help establish whether such layers were sufficiently thick to provide support for pile foundations. Initial tests with the dynamic test apparatus were unsuccessful due to hydraulic fluid leakage past the piston seals of the lift cylinders. Upon disassembly, it was discovered that the piston seals were step-cut metal rings similar to those used in automobile engines. The seals were replaced with rubber O-rings, which operated satisfactorily. After a number of blows with the repaired hammer, it was obvious that significant penetration could not be obtained beyond that obtained with the static test apparatus. Core samples in the area indicated that, in this locality, refusal with the static penetrometer occurred in dense gravels of substantial depth. Further testing with the dynamic apparatus was discontinued.

APPENDIX B: POINT RESISTANCE AND SKIN FRICTION DATA

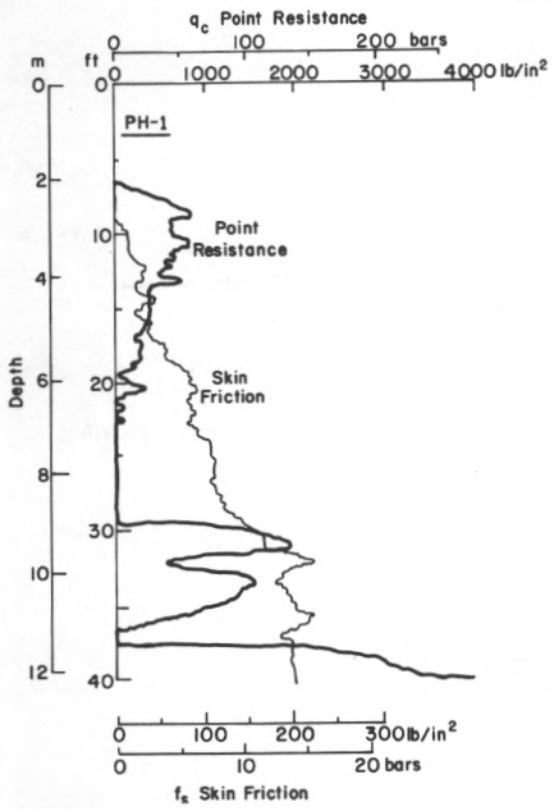

Figure B1. Point resistance and skin friction profiles, site PH-1.

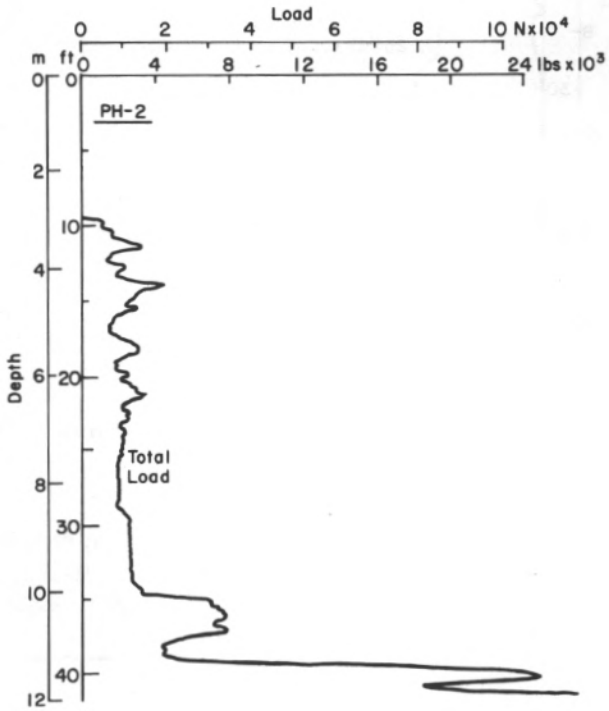

Figure B2. Point resistance and skin friction profiles, site PH-2.

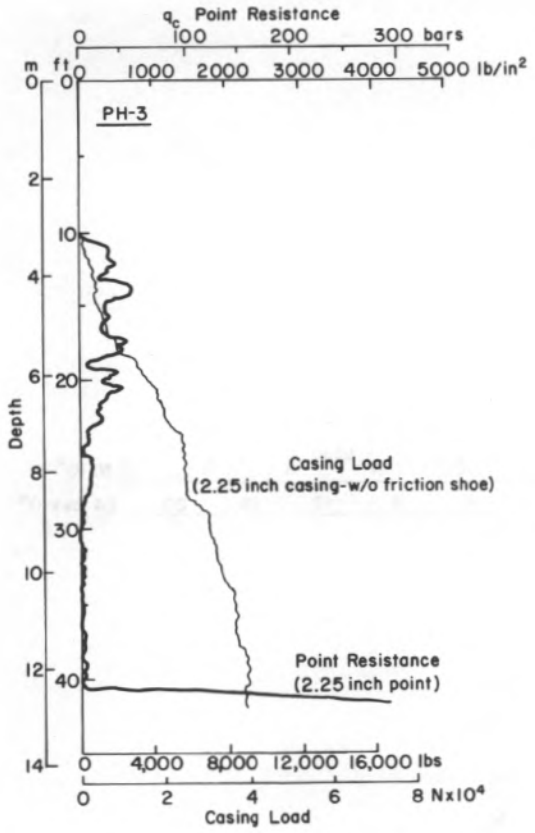

Figure B3. Point resistance and skin friction profiles, site PH-3.

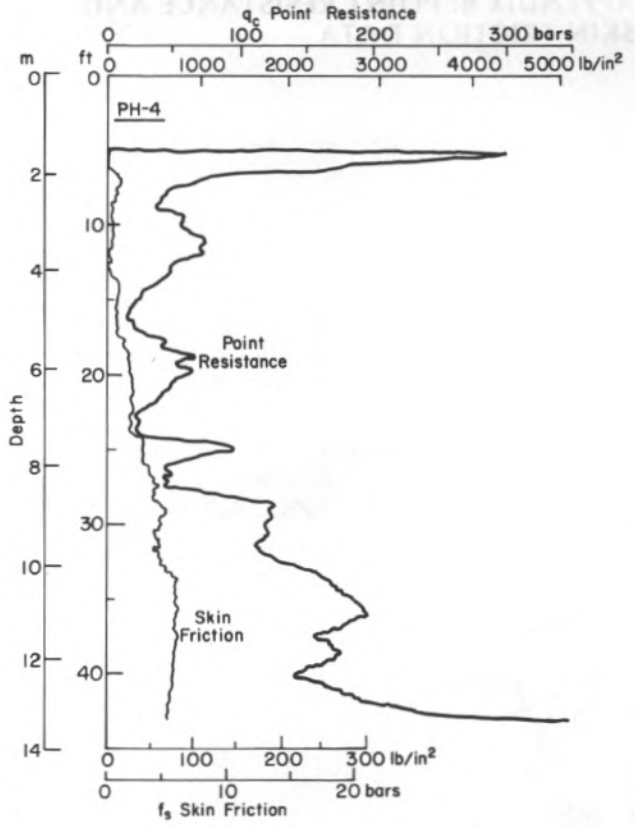

Figure B4. Point resistance and skin friction profiles, site PH-4.

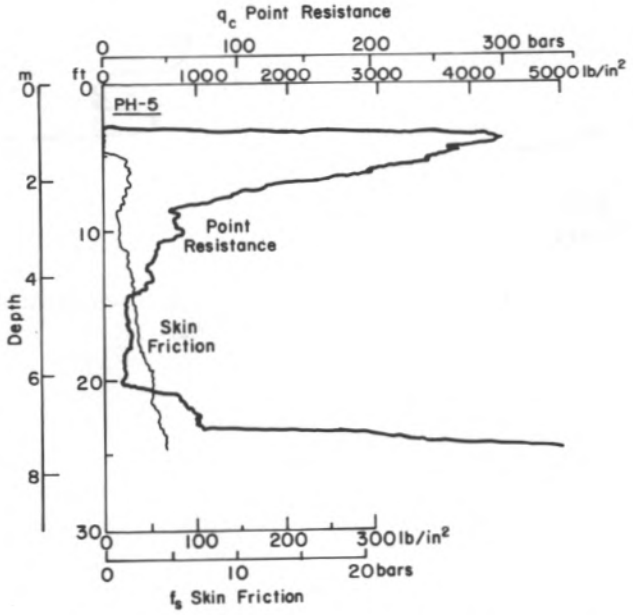

Figure B5. Point resistance and skin friciton profiles, site PH-5.

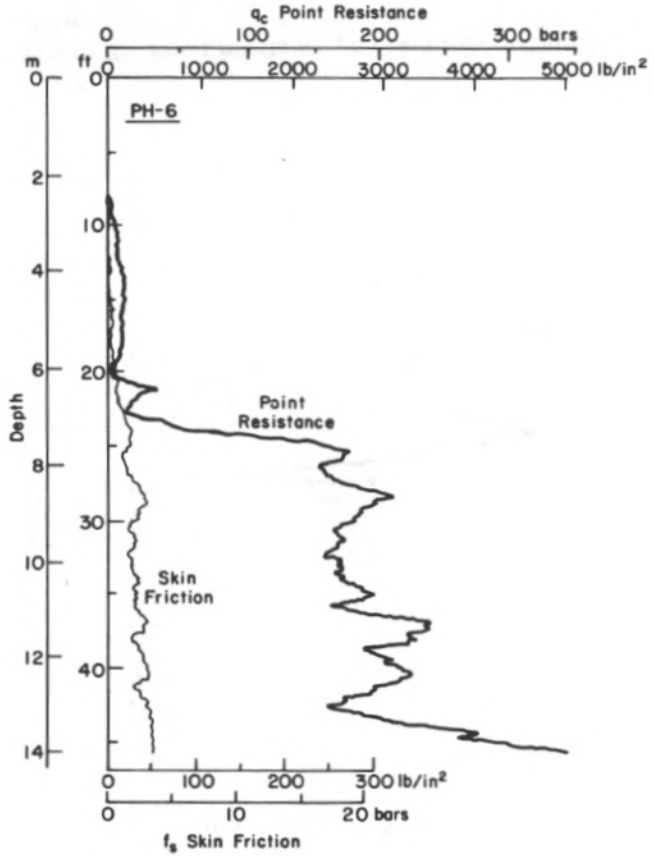

Figure B6. Point resistance and skin friction profiles, site PH-6.

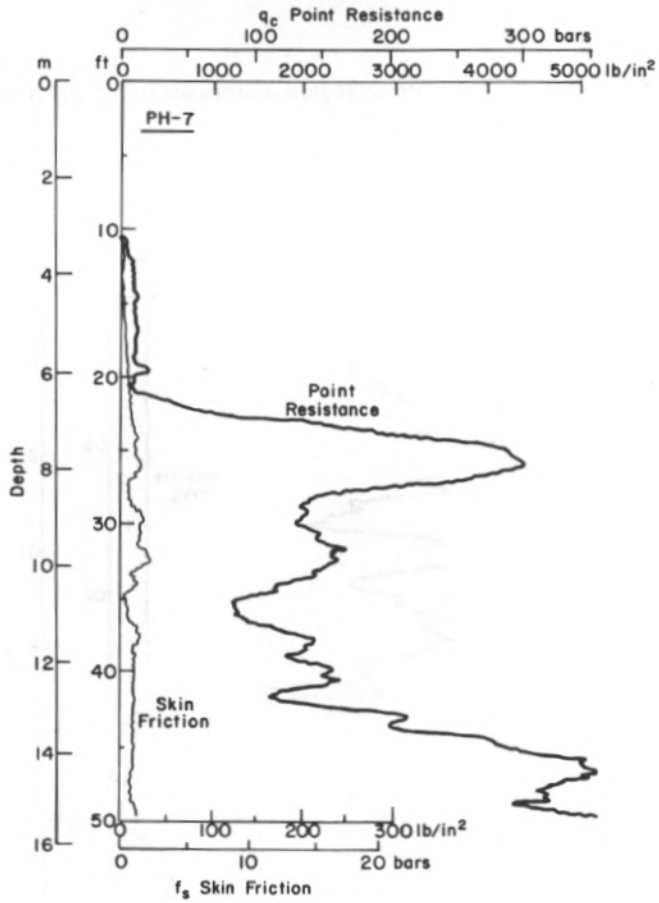

Figure B7. Point resistance and skin friction profiles, site PH-7.

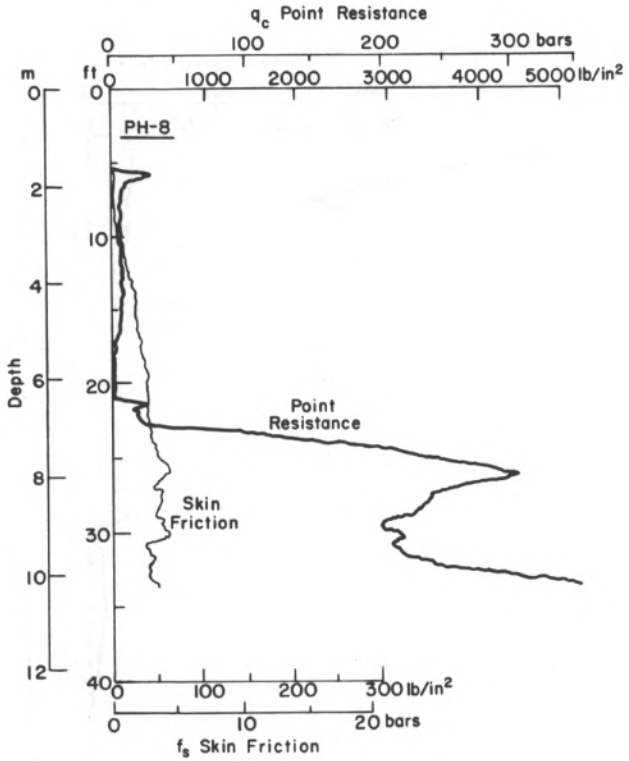

Figure B8. Point resistance and skin friction profiles, site PH-8.

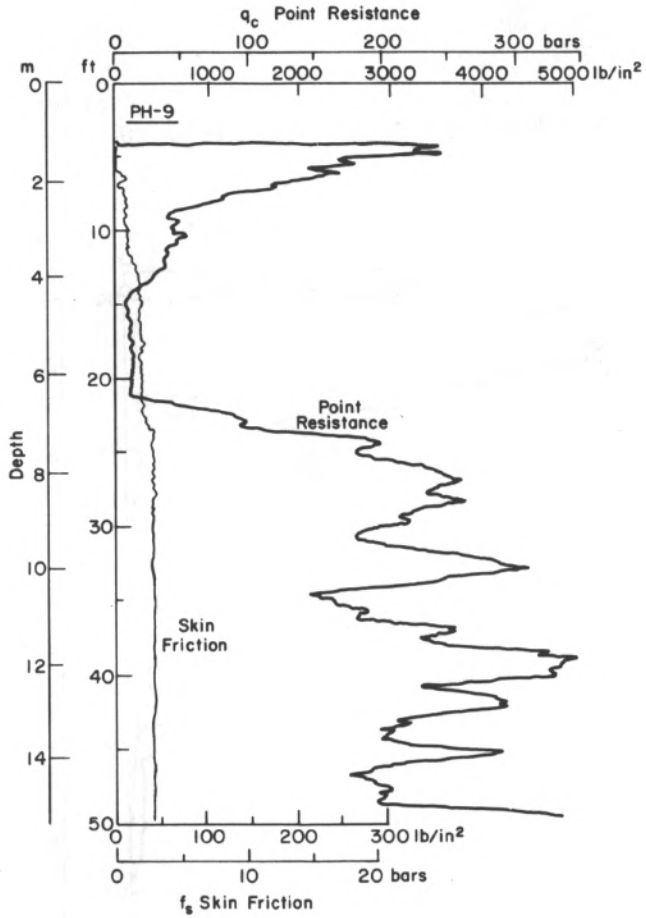

Figure B9. Point resistance and skin friction profiles, site PH-9.

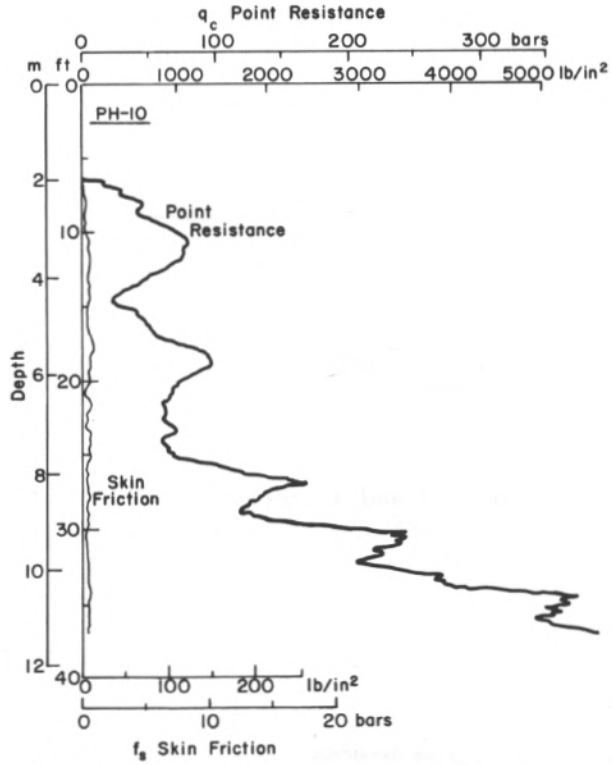

Figure B10. Point resistance and skin friction profiles, site PH-10.

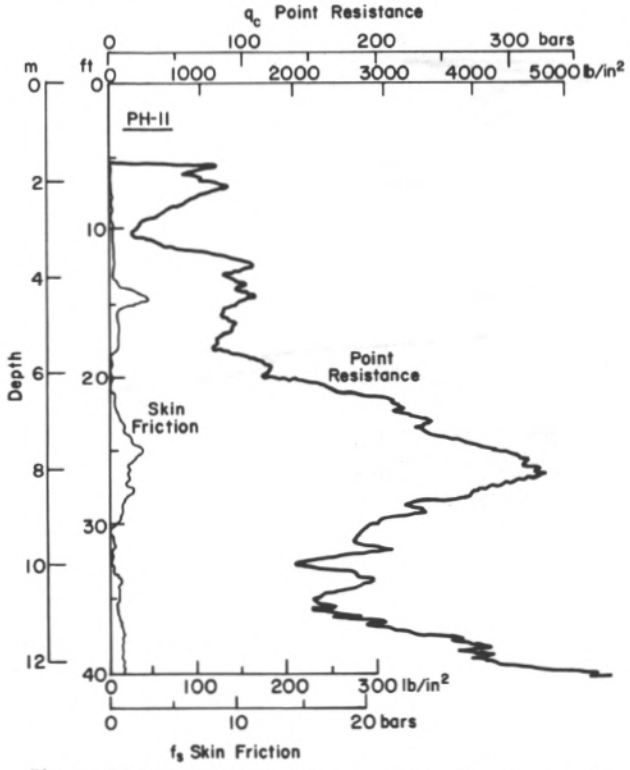

Figure B11. Point resistance and skin friction profiles, site PH-11.

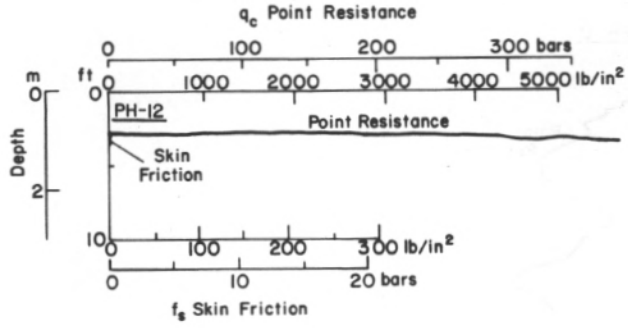

Figure B12. Point resistance and skin friction profiles, site PH-12.

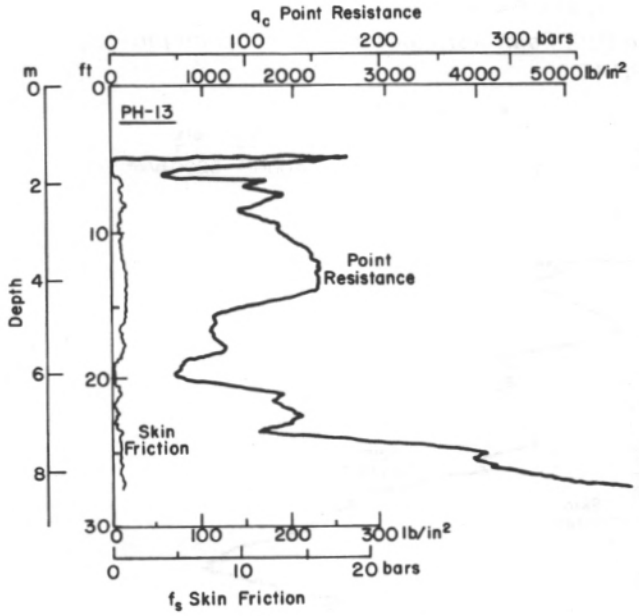

Figure B13. Point resistance and skin friciton profiles, site PH-13.

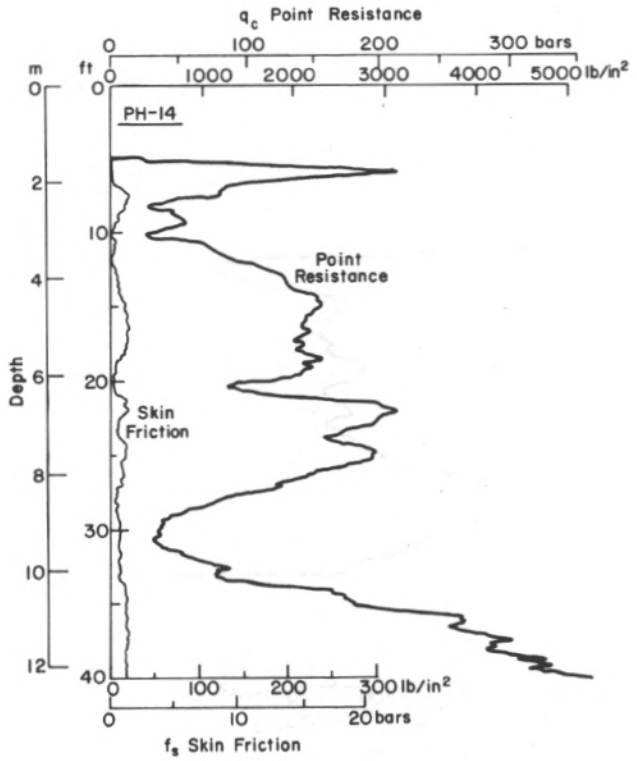

Figure B14. Point resistance and skin friction profiles, site PH-14.

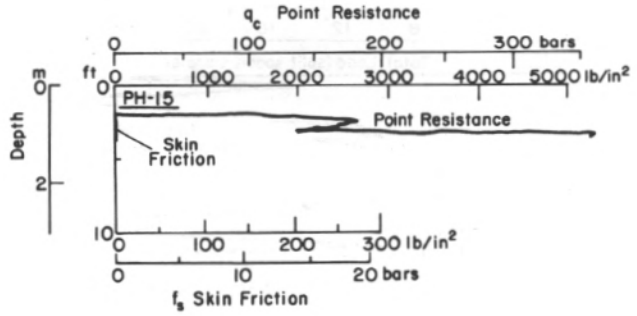

Figure B15. Point resistance and skin friction profiles, site PH-15.

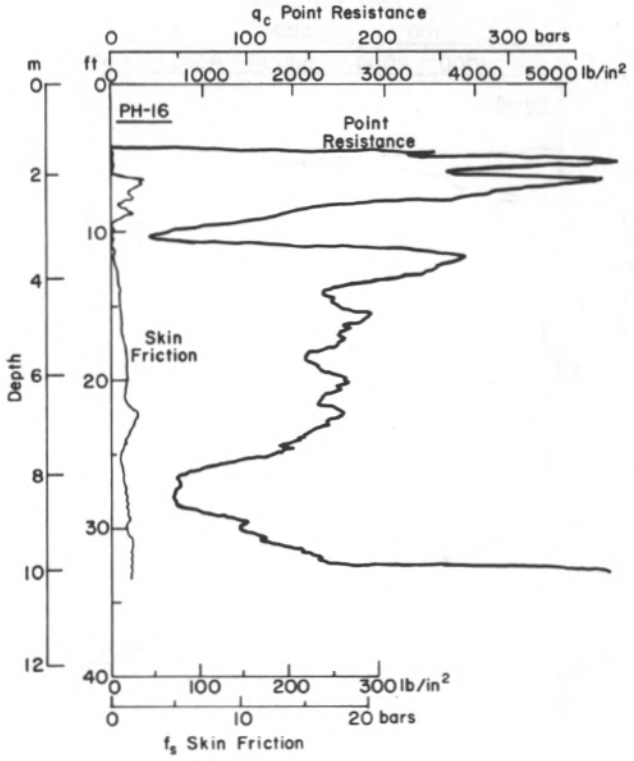

Figure B16. Point resistance and skin friction profiles, site PH-16.

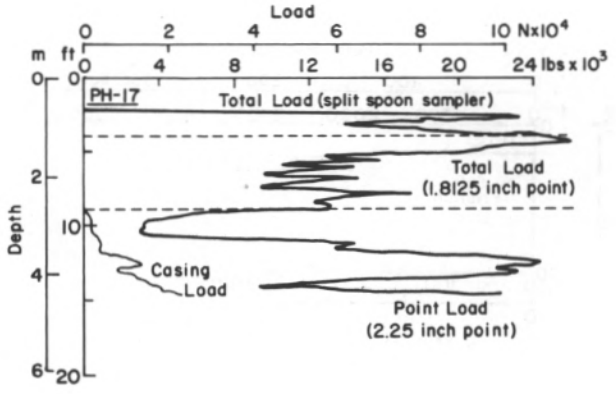

Figure B17. Point resistance and skin friction profiles, site PH-17.

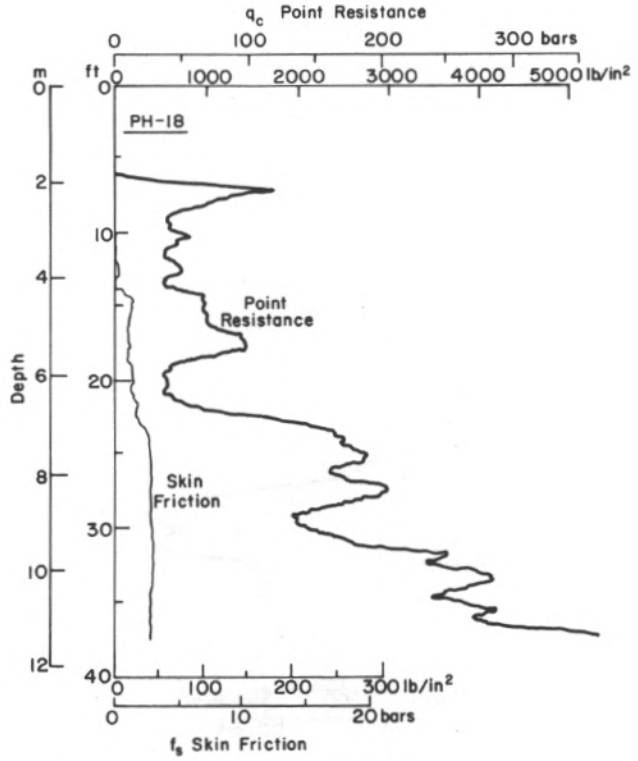

Figure B18. Point resistance and skin friction profiles, site PH-18.

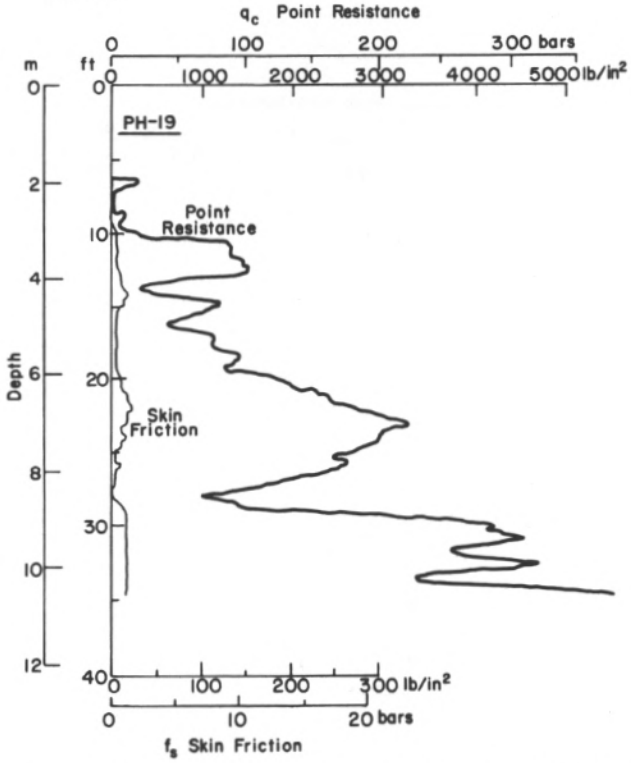

Figure B19. Point resistance and skin friction profiles, site PH-19.

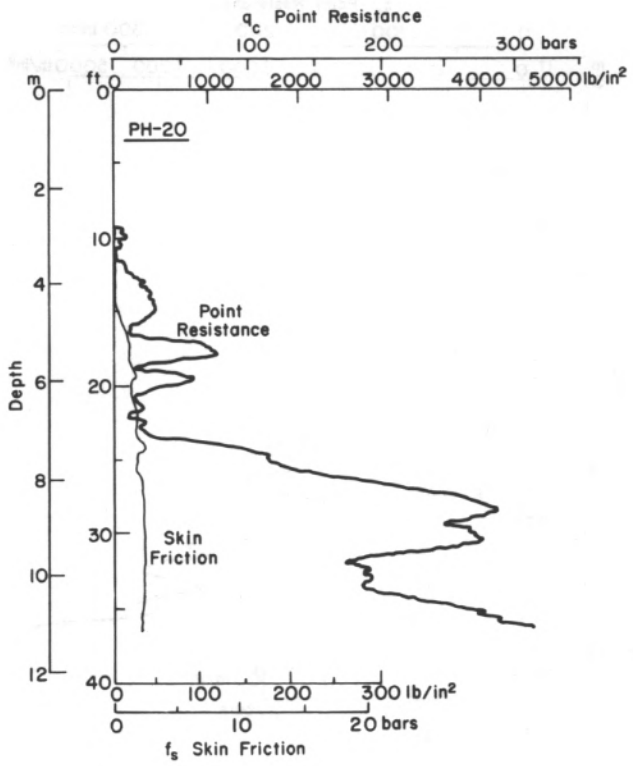

Figure B20. Point resistance and skin friction profiles, site PH-20.

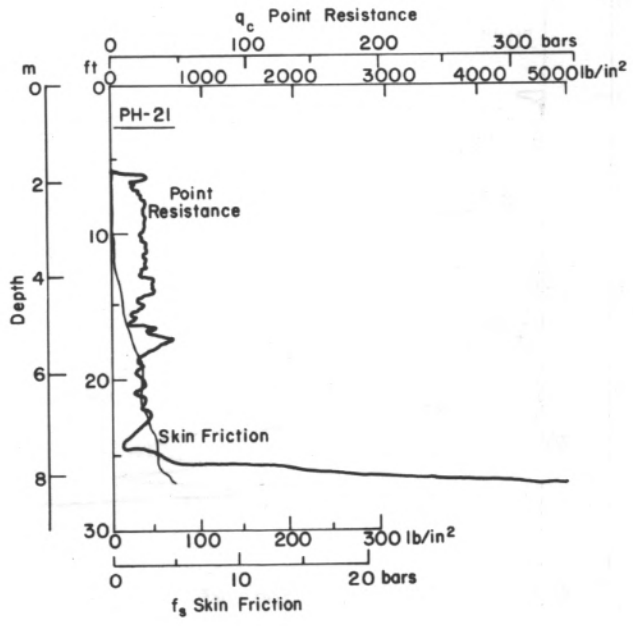

Figure B21. Point resistance and skin friction profiles, site PH-21.

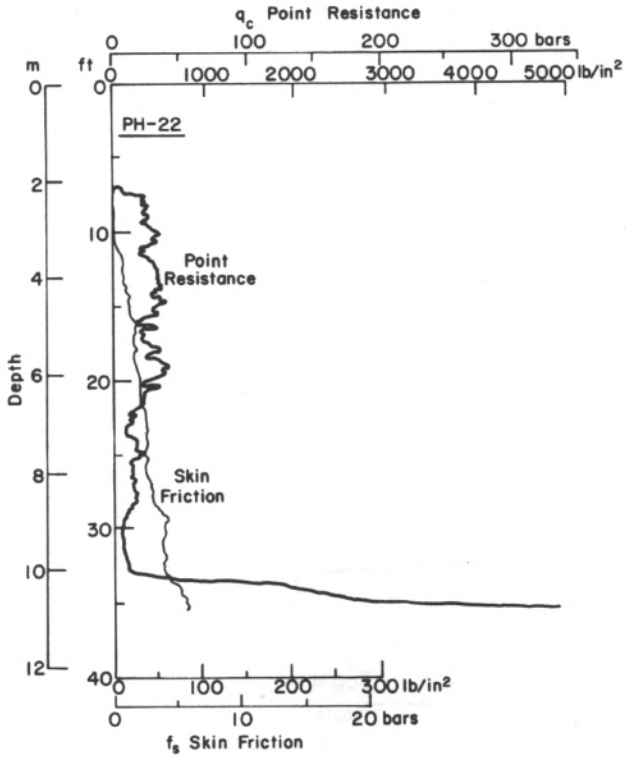

Figure B22. Point resistance and skin friction profiles, site PH-22.

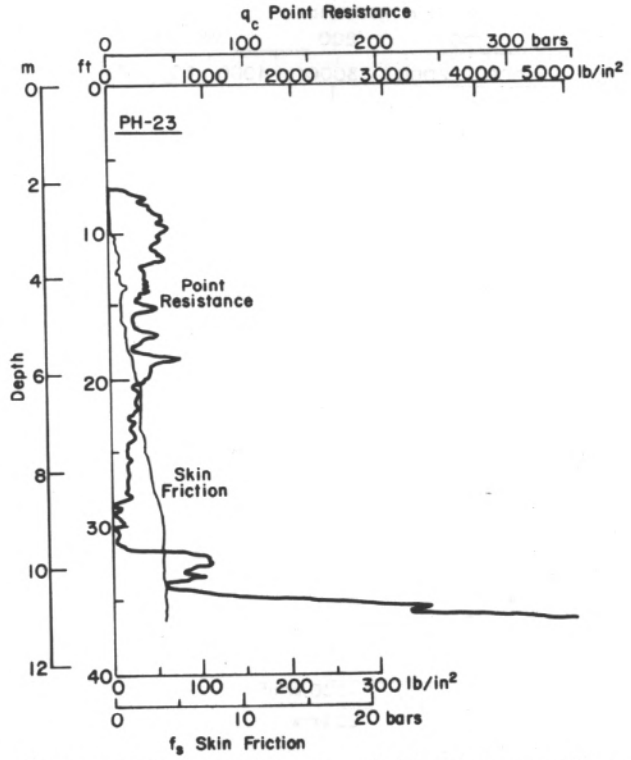

Figure B23. Point resistance and skin friction profiles, site PH-23.

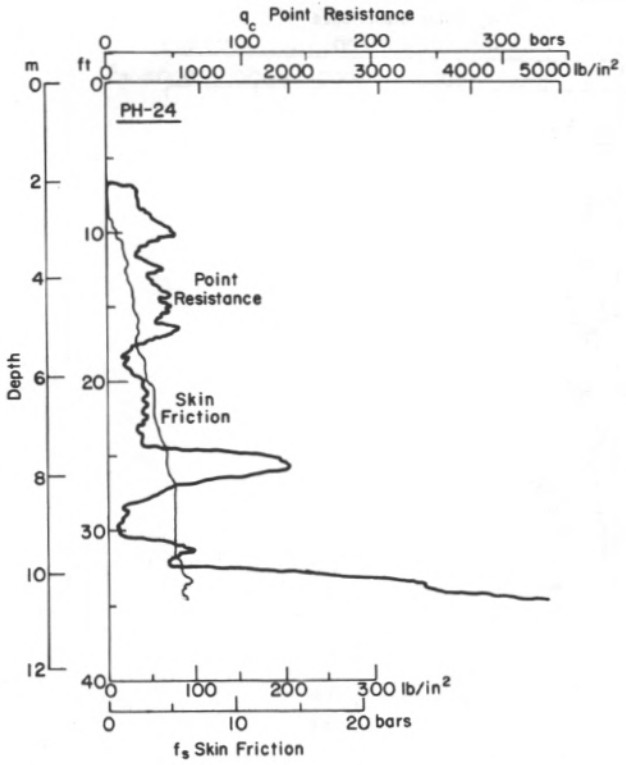

Figure B24. Point resistance and skin friction profiles, site PH-24.

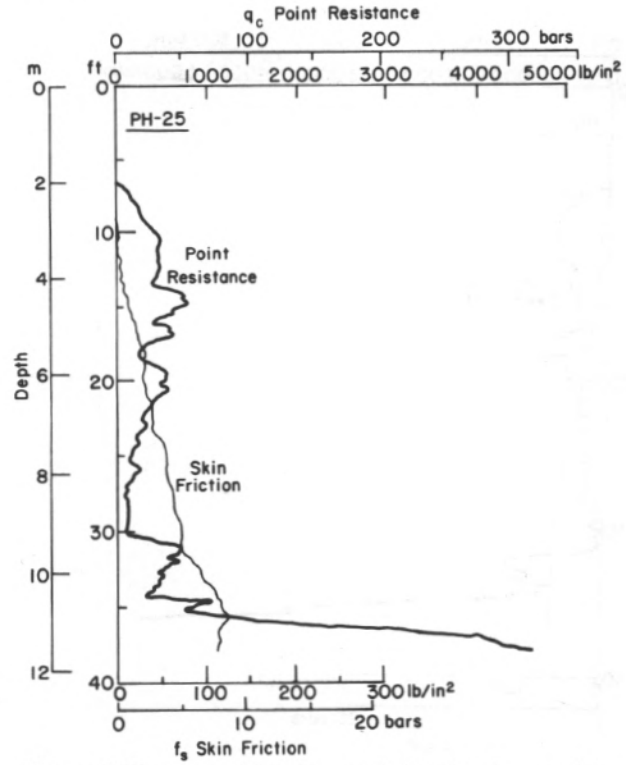

Figure B25. Point resistance and skin friction profiles, site PH-25.

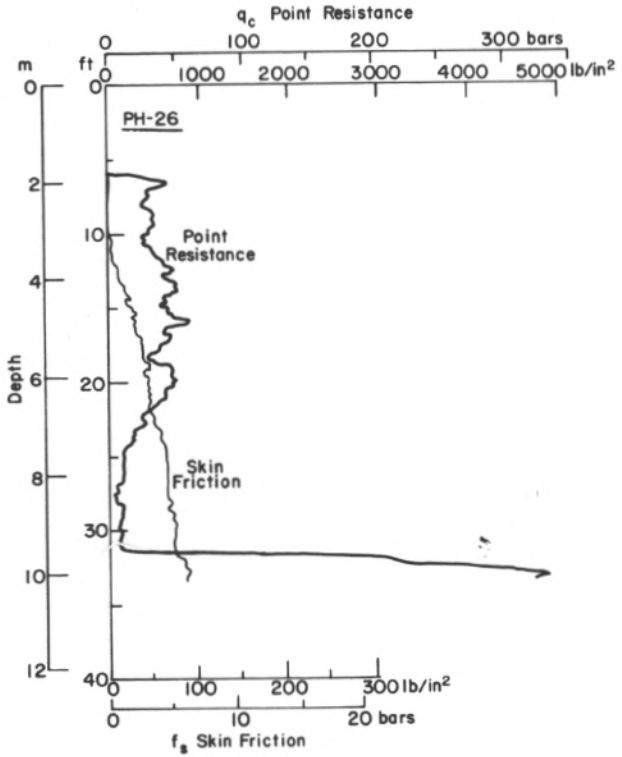

Figure B26. Point resistance and skin friction profiles, site PH-26.

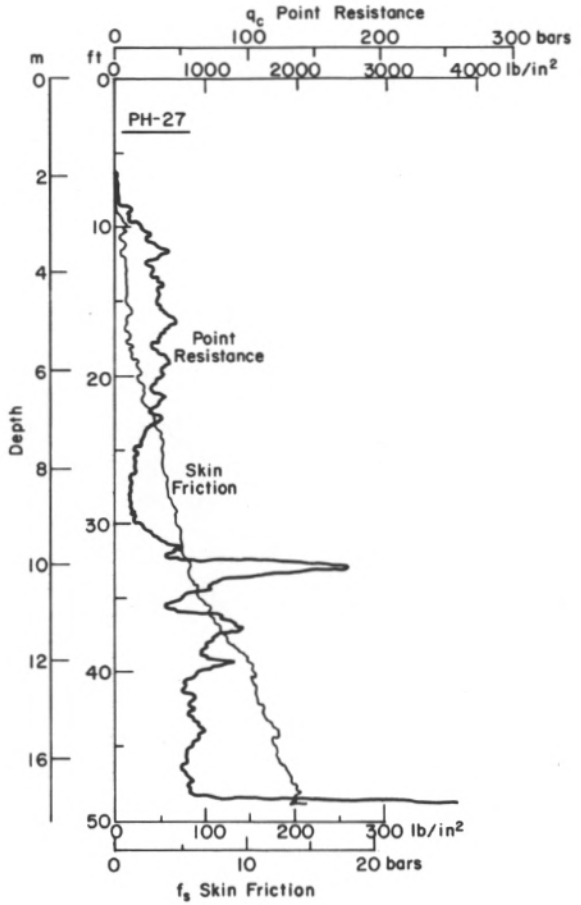

Figure B27. Point resistance and skin friction profiles, site PH-27.